

Intensification of decadal and multi-decadal sea level variability in the western tropical Pacific during recent decades

Weiqing Han · Gerald A. Meehl · Aixue Hu · Michael A. Alexander · Toshio Yamagata · Dongliang Yuan · Masayoshi Ishii · Philip Pegion · Jian Zheng · Benjamin D. Hamlington · Xiao-Wei Quan · Robert R. Leben

Received: 26 May 2013 / Accepted: 16 September 2013 / Published online: 2 October 2013
© Springer-Verlag Berlin Heidelberg 2013

Abstract Previous studies have linked the rapid sea level rise (SLR) in the western tropical Pacific (WTP) since the early 1990s to the Pacific decadal climate modes, notably the Pacific Decadal Oscillation in the north Pacific or Interdecadal Pacific Oscillation (IPO) considering its basin wide signature. Here, the authors investigate the changing patterns of decadal (10–20 years) and multidecadal (>20 years) sea level variability (global mean SLR removed) in the Pacific associated with the IPO, by analyzing satellite and in situ observations, together with reconstructed and reanalysis products, and performing ocean and atmosphere model experiments. Robust intensification is detected for both decadal and multidecadal sea level variability in the WTP since the early 1990s. The IPO intensity, however, did not increase and thus cannot explain the faster SLR. The observed, accelerated WTP SLR results from the

combined effects of Indian Ocean and WTP warming and central-eastern tropical Pacific cooling associated with the IPO cold transition. The warm Indian Ocean acts in concert with the warm WTP and cold central-eastern tropical Pacific to drive intensified easterlies and negative Ekman pumping velocity in western-central tropical Pacific, thereby enhancing the western tropical Pacific SLR. On decadal timescales, the intensified sea level variability since the late 1980s or early 1990s results from the “out of phase” relationship of sea surface temperature anomalies between the Indian and central-eastern tropical Pacific since 1985, which produces “in phase” effects on the WTP sea level variability.

Keywords Decadal · Multidecadal · Sea level · Pacific decadal variability · Indian Ocean warming

W. Han (✉) · J. Zheng
Department of Atmospheric and Oceanic Sciences, University of Colorado, UCB 311, Boulder, CO 80309, USA
e-mail: weiqing.han@colorado.edu

G. A. Meehl · A. Hu
Climate and Global Division, National Center for Atmospheric Research, Boulder, CO, USA

M. A. Alexander · P. Pegion · X.-W. Quan
Earth System Research Laboratory, NOAA, Boulder, CO, USA

T. Yamagata
Application Laboratory, Japan Agency for Marine-Earth Science and Technology, Yokohama, Japan

D. Yuan
Institute of Oceanology, Chinese Academy of Sciences, Qingdao, People’s Republic of China

M. Ishii
Meteorological Research Institute, 1-1, Nagamine, Tsukuba, Ibaraki 305-0052, Japan

J. Zheng
Ocean University of China, Qingdao, People’s Republic of China

B. D. Hamlington · R. R. Leben
Department of Aerospace Engineering Sciences, Colorado Center for Astrodynamics Research, University of Colorado, Boulder, CO, USA

1 Introduction

Decadal prediction is emerging as a new priority in climate research, due to its significant societal impacts and the need to adapt to climate change (Goddard et al. 2009; Hurrell et al. 2009; Meehl et al. 2009). As an essential component of decadal prediction, predicting decadal sea level variability, particularly at the local and regional level, has large societal demand (Milne et al. 2009; Church et al. 2011; Leuliette and Willis 2011; Nicholls 2011). Skillful predictions, however, rely critically on our understanding of how and why the sea level has varied on decadal timescales, and how the variations have evolved with time. In this paper, “decadal” refers to 10–20 year variability and “multidecadal”, >20 year variability.

1.1 Background

Satellite observations show that the highest rates of sea level rise (SLR) since the early 1990s have occurred in the western tropical Pacific (WTP), where sea level rose at a rate of >9 mm year⁻¹ from 1993 to 2010, which is nearly 3 times of the global mean rate (Cazenave and Llovel 2010; Nerem et al. 2010; Merrifield 2011; Fig. 1). Extensive studies have been carried out recently to explain this rapid regional SLR. By analyzing tide gauge data, Merrifield (2011) noticed an abrupt SLR in the WTP since the early 1990s relative to the preceding 40 years, and this abrupt rising rate is partly attributed to the global mean SLR by subsequent studies (Becker et al. 2012; McGregor et al. 2012; Merrifield et al. 2012; Zhang and Church 2012). After the global mean values are removed, the rates of WTP SLR reduce but still exhibit regional maxima, and a distinct spatial pattern emerges. The SLR in the WTP accompanies sea level fall in the eastern tropical basin, which is referred to as east–west dipole by Meyssignac et al. (2012). Both observational analysis and ocean modeling studies show that the steady intensification of the trade winds is the primary cause for the rapid WTP SLR since the early 1990s (Merrifield 2011; McGregor et al. 2012; Merrifield and Maltrud 2011; Nidheesh et al. 2012). Indeed, earlier studies have linked the WTP SLR and the eastern tropical Pacific sea level fall during 1993–2001 to decadal fluctuations of equatorial trade winds (e.g., Carton et al. 2005; Bindoff et al. 2007; Köhl et al. 2007; Timmermann et al. 2010).

The rapid WTP SLR, together with the easterly trade intensification since the early 1990s, is shown to be associated with decadal climate modes, particularly the decadal variability of El Niño–Southern Oscillation (ENSO), the Pacific Decadal Oscillation (PDO; Mantua et al. 1997; Minobe 1997; Zhang et al. 1997; Garreaud and Battisti 1999; and review papers by Alexander 2010 and Liu 2012)

and the Interdecadal Pacific Oscillation (IPO; Power et al. 1999; Folland et al. 2002; Meehl and Hu 2006; Power and Colman 2006; Randall et al. 2007). Zhang and Church (2012) performed multivariate statistical analysis, and showed that the large SLR in the WTP and fall in the eastern Pacific from 1993 to 2010 are correlated with the PDO (and thus IPO) and Multivariate ENSO indices. Merrifield et al. (2012) analyzed tide gauge data for the past 60 years and found significant correlations between the 5-year running mean WTP sea level variability (global mean removed) and PDO Index, and to a lesser degree, the Southern Oscillation Index. Feng et al. (2010) argued that the fast SLR in the WTP is associated with the spinup of the subtropical cells, which reversed their multidecadal weakening trends since the early 1990s (McPhaden and Zhang 2002, 2004). The spin up and spin down of the subtropical cells are associated with ENSO decadal variability (e.g., Kleeman et al. 1999). Meyssignac et al. (2012) analyzed reconstructed sea level from 1950 to 2009 and eight CMIP3 climate model solutions, and found that the 17 year reconstructed sea level trend patterns of 1959–1975 are similar to the 17 year satellite observed trends of 1993–2009, except that the SLR rates for 1993–2009 are higher in the WTP and there are some differences in detailed structures. The east–west sea level dipole variability generally follows the low-frequency Niño3.4 index. Similar dipole patterns were found in 17-year successive sea level trends in the majority of the climate model control runs with constant, preindustrial external forcing, and 4 out of the 8 models show significant correlations with low-frequency ENSO variability. Most of the twentieth century runs with varying external (natural and anthropogenic) forcing do not show significant differences with their respective control runs, even though the impact of external forcing could be seen in the peak frequency bands of the sea level variability spectra. Based on these analyses, the authors concluded that internal variability of the climate system associated with ENSO multidecadal variability dominates the 1993–2009 observed sea level trend patterns in the tropical Pacific.

In addition to the climate modes over the Pacific Ocean, satellite observations reveal coherent trend reversals of sea level and surface winds across the Indo-Pacific basin from 1993–2000 to 2000–2006, and the variability appears to occur earlier in the tropics (Lee and McPhaden 2008). These results demonstrate the close linkage between the Indian and Pacific ocean–atmosphere variability, and indicate the potential role of the tropics in determining the Indo-Pacific basin decadal climate. In contrast to the 1993–2010 sea level trend that represents multidecadal variability, the sea level trend reversal within the 1993–2006 period has a ~ 14 year timescale. Feng et al. (2010) analyzed a century long tide gauge record at

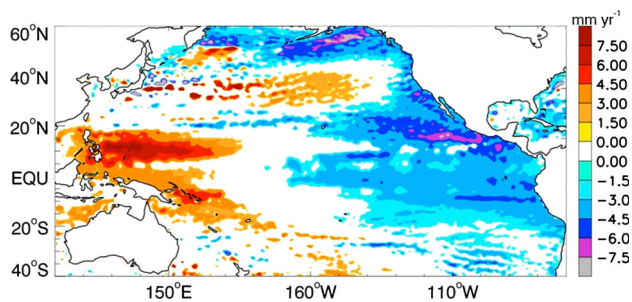


Fig. 1 Linear trends of sea surface height (SSH) (with global mean removed) from 1993 to 2010 from the AVISO multi-satellite gridded product, the same period as examined by Merrifield et al. (2012). Values that exceed 95 % significance are shown in *colors*, and those below 95 % significance are shown in *white*. Units: mm yr^{-1}

Fremantle, west coast of Australia, and showed increased energy of 8–16 year sea level variability since the late 1980s. They suggested that the increased 8–16 year energy results from the equatorial Pacific influence via the Indonesian Throughflow. Trenary and Han (2013) performed ocean general circulation model experiments, and showed intensified Pacific impact on Indian Ocean decadal sea level variability via the Throughflow after 1990 relative to the preceding two decades (their Fig. 13).

1.2 Present research

While previous studies have linked the intensification of WTP SLR and easterly trades since the early 1990s to multidecadal variability of the PDO, has the PDO intensity increased during recent decades to ensure the enhanced easterlies? While larger impacts of the equatorial Pacific on Indian Ocean decadal sea level variability since the late 1980s or early 1990s has been suggested, has the decadal sea level variability indeed intensified in the tropical Pacific Ocean? If yes, what are the causes?

The overall goal of this paper is to investigate the decadal and multidecadal intensifications of sea level variability in the tropical Pacific during recent decades, and to understand the causes. We will focus particularly on assessing the processes associated with ocean–atmosphere changes over the Indo-Pacific basin, given that the two basins are closely linked via both atmospheric bridge and oceanic connection, and that the Atlantic Multidecadal Oscillation has little effect on the tropical Indo-Pacific sea surface temperature (SST) variability (e.g., Sutton and Hodson 2005, their Fig. 1). Specifically, we first examine the evolution of the Pacific decadal mode, the IPO, and its changing relationship with the tropical Indian Ocean (TIO) SST. The IPO is quasi-symmetric ENSO-like interdecadal variability across the entire Pacific basin (e.g., Power et al. 1999; Meehl and Hu 2006), and is defined as the leading

empirical orthogonal function (EOF) of decadal–multi-decadal SST anomalies (SSTA) over the entire Pacific basin. The leading principle component (PC1) is referred to as the IPO index. Then, we assess the decadal and multi-decadal sea level variability patterns and their evolution associated with different phases of the IPO since the 1950s, and identify robust changes that have occurred during recent decades. Finally, we investigate the causes for the changes. The period of the 1950s-onward is chosen because both the observational based sea level and reanalysis product are available.

Here, we focus on the IPO instead of PDO and ENSO because IPO is the basin-wide Pacific decadal climate mode, whereas PDO primarily represents North Pacific climate variability, and ENSO is dominated by interannual variability (see Sect. 3.1 for further discussion). It has been suggested that the IPO has interdecadal modulation on interannual ENSO events (e.g., Power et al. 1999), and the PDO can be regarded as the North Pacific manifestation of the IPO (e.g., Folland et al. 2002; Meehl and Hu 2006). It is debatable, however, whether IPO can be confidently treated as an independent climate mode to ENSO (e.g., Trenberth et al. 2007). The indices of IPO, PDO and decadal variability of ENSO are all highly correlated (e.g., Alexander et al. 2002; Newman et al. 2003; Deser et al. 2004; Schneider and Cornuelle 2005; Vimont 2005; Zhang and Church 2012), and their correlations are further examined in Sect. 3.1. This study has important implications for decadal prediction, which is a challenging task because decadal climate variability is determined not only by natural internal variability of the climate system, but also affected by external natural and anthropogenic forcing, and both may contribute to the skill of decadal forecast (e.g., Hoerling et al. 2011; Solomon et al. 2011).

2 Datasets and models

We use a combined approach that integrates observational analyses with model experiments. Both ocean and atmosphere model experiments are performed.

2.1 Datasets and processing

To document the basin-wide ocean–atmosphere signatures, we analyze ocean–atmosphere variables from the following datasets: weekly multi-satellite merged sea surface height (SSH) anomalies from the French Archiving, Validation, and Interpolation of Satellite Oceanographic Data (AVISO) project (Ducet et al. 2000) available since October 1992, monthly HadiSST (Rayner et al. 2006), Hurrell SST (Hurrell et al. 2008), and Kaplan SST (Kaplan et al. 1998) since 1870,

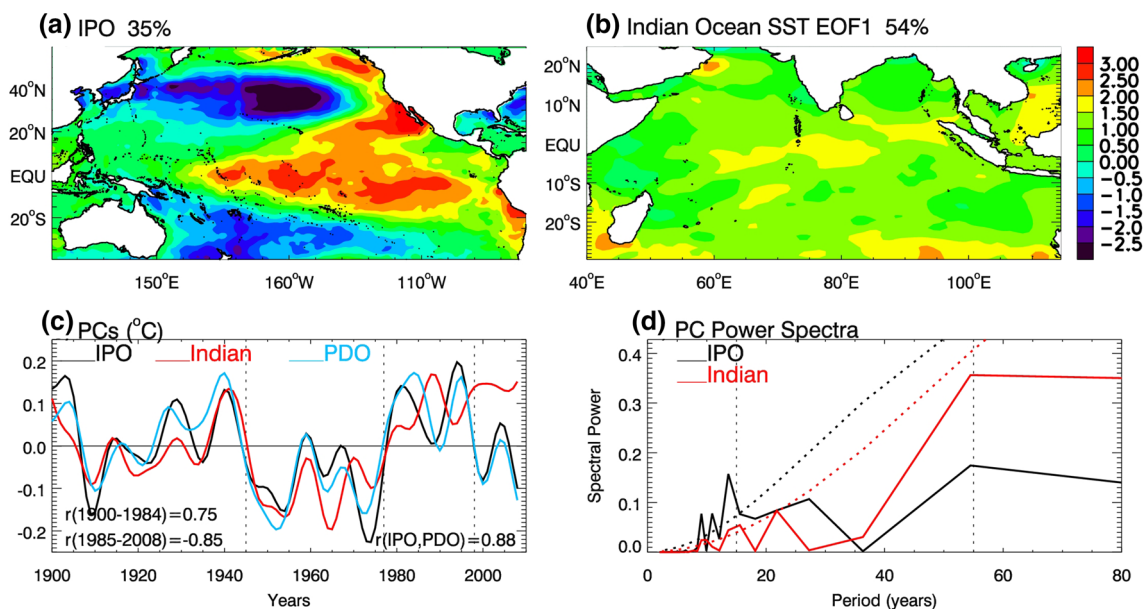


Fig. 2 **a** The leading EOF of SST for the Pacific Ocean, based on 8 year lowpass filtered monthly HadISST from 1900 to 2008, which represents the IPO spatial pattern and explains 35 % variance. The monthly SST data from 1870 to 2012 are first detrended and demeaned, and then the Lanczos lowpass filter with half power point placed at 8 year period is applied. The filtered SST from 1900 to 2008 is chosen to perform the EOF analysis. The 2009–2012 data are excluded to remove the 8 year lowpass filter's endpoint effect. **b** Same as (a) but for the Indian Ocean SST leading EOF, which

explains 54 % variance. **c** The leading PC (PC1) of 8 year lowpassed SST for the Pacific (*black curve*), Indian Ocean (*red*), and North Pacific ($>20^{\circ}\text{N}$; *blue*). The *black* and *blue* curves are defined as IPO and PDO indices. Units: $^{\circ}\text{C}$. **d** Variance spectra of IPO index (*black solid curve*) and Indian Ocean SST PC1 (*red solid curve*), and their corresponding 95 % significance levels (*dashed lines*). Units: $^{\circ}\text{C}^2$ (cycles year) $^{-1}$. Both Hurrell SST and Kaplan SST are analyzed, and they provide similar results, even though there are some quantitative differences

the cross-calibrated multiplatform (CCMP) satellite surface winds (Atlas et al. 2008) available since July 1987, satellite derived outgoing longwave radiation (OLR; Liebmann and Smith 1996) available since 1979, and Wave- and Anemometer-Based Sea Surface Wind (WASWinds; Tokinaga and Xie 2011). To extend the sea level analysis back to the 1950s, we also analyze the upper-700 m thermosteric sea level from 1945 to 2010 calculated from updated version of Ishii and Kimoto (2009) temperature data, and sea level reconstructed specifically for the Pacific Ocean from 1950 to 2009 (Hamlington et al. 2011). The justification of using the upper-ocean thermosteric sea level is that it is the dominant component of the observed sea level variability, although salinity may also play some role at regional scales (Wunsch et al. 2007; Köhl and Stammer 2008; Lombard et al. 2009; Meyssignac et al. 2012; Nidheesh et al. 2012).

In addition to the observed and reconstructed datasets, we also analyze surface winds from the European Centre for Medium-Range Weather Forecasts (ECMWF) Reanalysis Interim (ERA-Interim) data available since 1989 (Simmons et al. 2007), the ECMWF operational ocean analysis/reanalysis system (ORA-S3) available for 1959–2009 (Balmaseda et al. 2008), and the National Centers for Environmental Prediction (NCEP; Kalnay et al. 1996) available since 1948. This multiple datasets approach aims

to identify signals that exceed cross-dataset differences, and thus increase confidence in our analysis.

To isolate decadal-multidecadal variability signals, a Lanczos lowpass filter (Duchon 1979) with half power placed at 8 year period is used. The response curve of the 8 year lowpass filter retains $\sim 90\%$ of the amplitude at 10 year period and almost full amplitudes for longer periods, which essentially retains the signals with periods of 10 years and longer. The 8 year lowpassed filter has been used to investigate the Pacific decadal variability by previous studies (e.g., Deser et al. 2012). A Lanczos 8–20 year bandpass filter is used to isolate decadal signals.

2.2 Ocean model and experiment

To isolate the effects of winds in driving the Pacific sea level pattern, a Linear continuously stratified Ocean Model (LOM; McCreary 1981) driven solely by surface wind stress is used. The LOM has been applied to the Indian, Atlantic and Indo-Pacific basins (e.g., Han 2005; Han et al. 2008, 2010; Trenary and Han 2013). In this paper, it is set up for Indo-Pacific basin (30°E – 290°E , 55°S – 55°N) with $0.33^{\circ} \times 0.33^{\circ}$ horizontal grids. The solution is well converged using the first 15 baroclinic modes. The LOM was first spun up for 30 years using ECMWF ORA-S3 monthly

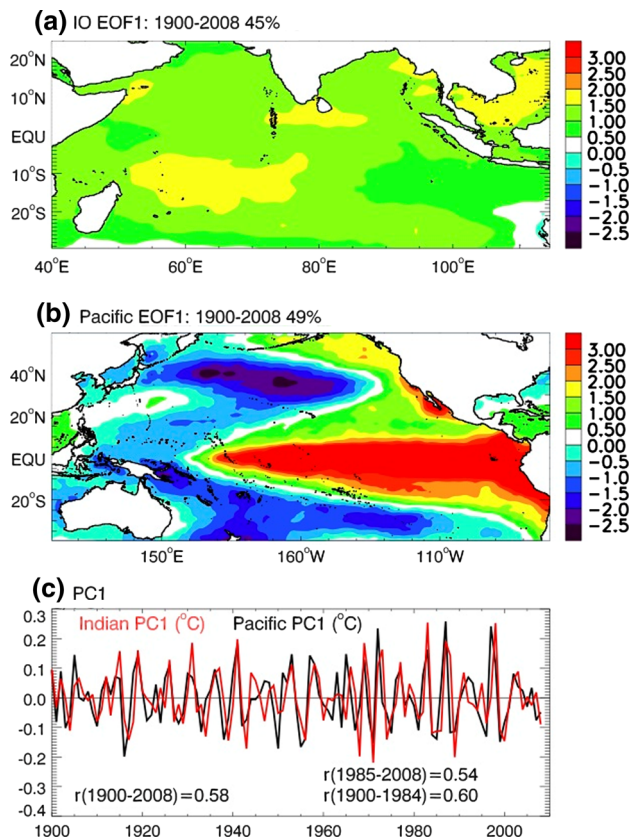


Fig. 3 **a** Tropical Indian Ocean (TIO) interannual SST EOF1 for the 1900–2008 period, based on 8 year highpassed HadiSST data from 1870 to 2012; the mean and linear trend for 1870–2012 are removed before the filtering; then we choose 1900–2008 period to perform EOF analysis (the 2009–2012 data are excluded to remove the filter's endpoint effect); It explains 45 % variance; **b** same as **(a)** but for the Pacific EOF1, which is the ENSO mode and explains 49 % variance; **c** PC1 of SST EOF1 for the Pacific (black) and TIO (red). The correlation between the two curves is 0.58 for 1900–2008 and 0.60 for 1900–1984, with both >99 % significance. Their correlation coefficient is 0.54 for 1985–2008 (>90 % significance), which does not change sign relative to the pre-1985 period. Units for the PCs: °C

wind stress of 1959. Restarting from year 30, the model was integrated forward using monthly ORA-S3 wind stress forcing from 1959 to 2009.

2.3 Atmospheric models and experiments

To assess the effect of TIO warming since the 1950s, we perform two idealized experiments using the National Aeronautics and Space Administration Seasonal-to-Interannual Prediction Project (NSIPP) Atmospheric General Circulation Model (AGCM) with horizontal grids of $3.75^\circ \times 3^\circ$ and 34 vertical levels (see Schubert et al. 2004 for details). One is forced by the Hurrell et al. (2008) global monthly SST climatological annual cycle of 1971–2000 with a 0.5°C anomaly uniformly added to 10°S – 10°N and

linearly ramped to zero from 10 – 20°S and 10 – 20°N . This solution is based on the observed warming rates in most regions of the global tropical oceans since the 1950s (see Sect. 3.2.3), and is referred to as AGCM_0.5C. The other is the same as AGCM_0.5C except for adding an additional 0.5°C warming to the TIO from the western boundary to 110°E with linear ramping to zero at 130°E . This experiment is based on the observations showing that the TIO warms faster than the tropical Pacific and Atlantic (Sect. 3.2.3). This solution is referred to as AGCM_TIO1.0C. Both experiments were run for 50 years, and the last 45 years results are analyzed, and their average represents the 45-member ensemble mean. The difference between the two experiments, (AGCM_TIO1.0C–AGCM_0.5C), estimates the 0.5°C warmer TIO and is referred to as AGCM_TIO0.5C. Conversely, the–AGCM_TIO0.5C measures the effect of TIO 0.5°C cooling.

To understand the role of tropical versus global SST in generating the Pacific basin-wide surface winds that drive the spatial patterns of sea level variability, we analyze the results from two experiments using the National Center for Atmospheric Research (NCAR) Community Atmospheric Model version 3 (CAM3) at T85 (equivalent to $1.48^\circ \times 1.48^\circ$) horizontal resolution. Two experiments are analyzed: the 5-member ensemble of Global Ocean Global Atmosphere (GOGA) experiment for 1950–2008, which is forced by global time-varying SSTs of Hurrell et al. (2008) and referred to as AGCM_GOGA, and the 5-member ensemble of Tropical Ocean Global Atmosphere (TOGA) forced by tropical (20°N – 20°S) monthly SSTs from 1950 to 2008 and SST climatological seasonal cycle polewards of 30° , with linear interpolation between 20° and 30° (referred to as AGCM_TOGA). The two experiments were performed by the Climate Variability Working Group at NCAR (Deser and Phillips 2009), and the model physics and performance were reported by previous studies (e.g., Collins et al. 2006; Deser et al. 2006; Hack et al. 2006; Hurrell et al. 2006).

While the AGCM experiments are straightforward in assessing regional SST effects on atmospheric circulation, we are aware of their limitations. One key issue is that on interannual timescales, the TIO warming can be a response to remote forcing from the Pacific El Niño, which causes anomalous subsidence over the TIO, reduces convection, increases shortwave radiation and thus induces warming (Kumar and Hoerling 1998; Kumar et al. 2005; Wu et al. 2006; Deser and Phillips 2006; Copsey et al. 2006; Xie et al. 2009). The observed steady warming over the Indian Ocean since the 1950s, however, is attributed to increased greenhouse gases instead of resulting from the Pacific influence, by analyzing the results from eleven CMIP3 climate models (e.g., Du and Xie 2008). Consequently, our AGCM experiments, particularly the AGCM_TIO0.5C,

Table 1 The 17 year cooling/warming rates of IPO index for four representative time spans associated with IPO multidecadal phase transition periods (Fig. 2c), and the corresponding sea level changing rates (with the global mean SLR removed) since 1959 from the upper

| IPO phase transition time span | IPO phase transition rate ($^{\circ}\text{C year}^{-1}$) | WTP thermo. sea level rate (mm year^{-1}) | CETP thermo. sea level rate (mm year^{-1}) | WTP ORA-S3 sea level rate (mm year^{-1}) | CETP ORA-S3 sea level rate (mm year^{-1}) |
|--------------------------------|--|--|---|---|--|
| 1940–1956 | −0.0170 | | | | |
| 1959–1975 | −0.0142 | 2.0 | −1.5 | 1.9 | −3.0 |
| 1976–1992 | 0.0033 | −1.5 | 1.4 | −1.5 | 0.5 |
| 1993–2008 (1993–2009) | −0.0145 | 5.2 | −1.5 | 6.6 | −0.7 |

An exception is for the last period, which is 16 year long from 1993 to 2008 for IPO index, because the 2009 data are excluded to remove the 8 year lowpass filter's end point effect. The three 17 year sea level trend periods are the same as those of Meyssignac et al. (2012)

will help to provide insight into the effects of TIO warming on Indo-Pacific basin climate.

3 Results

In this section, we first discuss the IPO evolution since 1900, point out its distinct decadal and multidecadal timescales, and examine its changing relationship with TIO SST variability as well as their association with the 1993–2010 sea level trend (Sect. 3.1). Then we assess the Pacific sea level variability patterns associated with multidecadal variability of IPO and TIO SST since the 1950s, identify the robust changes that have occurred during recent decades, particularly the rapid SLR in the WTP from 1993 to 2010, and understand the causes (Sect. 3.2). Finally, we examine the spatial patterns and temporal evolution of 10–20 year sea level variability associated with the IPO and TIO SST decadal variability, identify robust changes and understand the causes (Sect. 3.3).

3.1 The IPO and its changing relationship with TIO SST since 1900

The IPO spatial pattern (Fig. 2a) is ENSO-like and resembles that from previous studies (e.g., Power et al. 1999; Meehl and Hu 2006). The IPO is highly correlated with the PDO, with a correlation coefficient of 0.88 (>95 % significance) during 1900–2008 (Fig. 2c). It is also highly correlated with decadal-multidecadal variability (8 year lowpassed) of ENSO indices, with a correlation of 0.88 with NINO3.4 index for 1900–2008 and 0.89 with multivariate ENSO index (<http://www.esrl.noaa.gov/psd/enso/mei.txt/>) for 1900–2001. On multidecadal timescales, the IPO changes phases near 1925, 1945, 1977 and 1998. The first three phase changes are consistent with the well-documented PDO phase transitions in existing literatures

700 m thermosteric sea level and ECMWF ORA-S3 sea level averaged in the WTP (130°E–160°E, 15°S–15°N) and central-east tropical Pacific (CETP; 160°W–110°W, 15°S–15°N) regions

(e.g., Zhang et al. 1997; Mantua et al. 1997), and the most recent one near 1998 is discussed in Dai (2012). All the four-phase transitions are also shown in the monthly PDO index posted online (<http://jisao.washington.edu/pdo/>). Overlying on the multidecadal phase reversals, there are 10–20 year variability, as shown by the IPO index and its spectra (Fig. 2c, d, black lines). These timescales are consistent with the 10–20 year (e.g., Zhang et al. 1997) and 50–70 year (e.g., Minobe 1997) periods of the PDO.

The observed spatial pattern of sea level trends from 1993 to 2010 (Fig. 1) is associated with the multidecadal IPO (and thus PDO) phase transition from positive to negative, referred to as “cold transition” hereafter (Fig. 2a, c). This is consistent with the high correlation between the PDO index and WTP sea level variability found by previous studies (Sect. 1). Note that the 16 year trend of IPO index for 1993–2008 is $-0.0145\text{ }^{\circ}\text{C year}^{-1}$, which is smaller than the 16 year cooling rate of $-0.019\text{ }^{\circ}\text{C year}^{-1}$ for 1940–1955 and is comparable to the $-0.014\text{ }^{\circ}\text{C year}^{-1}$ 16 year cooling rate for 1959–1974, when IPO index changing from weakly positive to its negative minimum. The 17 year time spans used by Meyssignac et al. (2012) are also tested, and we obtain similar values (Table 1). These results suggest that even though the rapid SLR in the WTP since 1993 is associated with IPO cold transition, the IPO did not intensify comparing to the preceding decades and thus cannot fully explain the SLR acceleration.

Within each IPO multidecadal phase period, there are 10–20 year variations (Fig. 2c, d). The standard deviation (STD) of the IPO index within each IPO phase period (with the mean for this period removed) is $0.057\text{ }^{\circ}\text{C}$ for 1925–1945 positive phase (IPO+), $0.069\text{ }^{\circ}\text{C}$ for 1946–1977 IPO−, $0.062\text{ }^{\circ}\text{C}$ for 1978–1998 IPO+ and $0.055\text{ }^{\circ}\text{C}$ for 1999–2008 IPO−. Apparently, the 10–20 year IPO amplitudes did not increase since the early 1990s (also see Table 2), whereas there are indications of intensified influence from the equatorial Pacific on the

Table 2 Standard deviation (STD) of 10–20 year sea level anomalies averaged in the western tropical north Pacific (WTNP; 125°E–160°E, 0°N–15°N) and central- equatorial Pacific (CEQP; 170°E–130°W, 10°S–5°N) for different decades, together with the STD of 10–20 year IPO index for the same decades

| Decadal period | IPO | WTNP Thermo. | CEQP Thermo. | WTNP ORA-S3 | CEQP ORA-S3 |
|----------------|------|--------------|--------------|-------------|-------------|
| 1963–1976 | 0.08 | 1.12 | 1.09 | 1.80 | 2.17 |
| 1977–1990 | 0.05 | 1.31 | 1.18 | 1.32 | 1.27 |
| 1991–2005 | 0.06 | 2.84 | 2.71 | 2.63 | 2.59 |

To exclude the multidecadal signals associated with the IPO, the IPO index and sea level anomalies are calculated within each IPO multidecadal phase that overlaps with the sea level data period (1963–1977 IPO–, 1978–1998 IPO+ and 1999–2005 IPO–), with the mean of each period removed. The 8 year lowpassed thermosteric sea level and ECMWF ORA-S3 sea level data are used for the calculation. The first and last four years data are excluded to remove the filter's end point effect. Then we form a 43 year time series from 1963 to 2005 and perform the STD calculations for different decades with a 14 year interval (the last one is 15 years). Units: °C for IPO index and cm for sea level anomalies

Table 3 Correlation coefficients for sea level variability from the upper-700 m thermosteric sea level, IPO index, Indian Ocean SST PC1 and Nino3.4 SST

| | IPO | Indian Ocean SST PC1 | Nino3.4 |
|----------------|-------------------------|-------------------------|-------------------------|
| WTNP sea level | –0.72 (99 %; 1950–2006) | –0.48 (85 %; 1950–1984) | –0.87 (99 %; 1950–2006) |
| | | 0.76 (90 %; 1985–2006) | |
| CEQP sea level | | | 0.65 (90 %) |
| IPO | 1.0 (99 %; 1900–2008) | 0.75 (99 %; 1900–1984) | 0.88 (99 %; 1900–2008) |
| | | –0.85 (95 %; 1985–2008) | 0.83 (99 %; 1950–2006) |

All indices are based on 8 year lowpassed data, which include both decadal and multidecadal variability. The WTNP (125–160°E, 0–15°N) and CEQP (170°E–130°W, 10°S–5°N) are the two regions for calculating sea level anomalies and are shown in Figs. 14, 15. Only the correlation coefficients exceeding 85 % significance are shown. The % values in the parentheses show the significance level, and year ranges show the time span for calculating the correlation. The reduced degree of freedom due to the filter has been considered in the significance test (Livezey and Chen 1983)

eastern Indian Ocean during recent decades (Sect. 1). Ideally, we should perform 10–20 year bandpass filtering to isolate the 10–20 year signals; however, the filtered data will eliminate the entire period of the recent negative IPO phase since 1999 by excluding the filter's endpoint effects. Here, we use the STD of IPO index within each IPO multidecadal phase as an estimate of the 10–20 year IPO variability, because IPO index is dominated by ~14 year variability within each multidecadal phase (Fig. 2c, d).

One interesting change that has occurred during recent decades, which coincides with the WTP sea level intensification, is the relationship between the IPO and TIO SST (Fig. 2c, black and red curves). While the IPO and TIO SST indices co-vary on multidecadal timescales before 1998, they have opposite signs after 1998, with cold tropical Pacific corresponding to warm TIO (Fig. 2c). On decadal and multidecadal timescales, the IPO and basin-wide warming/cooling pattern of TIO SST (Fig. 2b) are positively correlated before 1985, with a correlation coefficient of 0.75 from 1900 to 1984 (Fig. 2c; Table 3). This warm/cold tropical Pacific corresponding to warm/cold TIO pattern resembles the interannual ENSO effects on TIO SST. While the El Niño events cause TIO warming, La Niña events cause TIO cooling (e.g., Nigam and Shen 1993; Klein et al. 1999; Kumar and Hoerling 2003; Liu and Alexander 2007). In addition, El Niño/La Niña can also warm/cool the south TIO through generating downwelling/upwelling oceanic Rossby waves by surface wind anomalies (e.g., Huang and Kinter 2002; Xie et al. 2002). Since 1985, however, the IPO and TIO SST are negatively correlated, with a correlation of –0.85 (Fig. 2c; Table 3). As we shall see below, this IPO/TIO SST changing relationship plays an important role in amplifying the WTP sea level variability.

Note that the changing relationship only occurs on decadal-multidecadal timescales. On interannual timescales, Pacific ENSO dominates the TIO SSTA throughout the 1900–2008 period, and their indices are positively correlated both before and after 1985 (Fig. 3). This is another reason for us to focus on the IPO decadal-multidecadal variability instead of ENSO, which is dominated by interannual variability and strongly affects TIO SSTA.

3.2 Multidecadal sea level acceleration in the WTP since 1993 and causes

3.2.1 Changes of multidecadal sea level variability patterns

The rapid WTP SLR since the early 1990s accompanies basin-wide sea level fall in the eastern Pacific, and weaker SLR in the central North Pacific near 30–45°N (Figs. 1, 4a). This satellite observed sea level trend pattern is associated with the IPO cold transition and is well reproduced by the upper 700 m thermosteric sea level from 1993 to 2009, albeit with some quantitative differences (Fig. 4b). Comparing the 17 year IPO warm transition period of 1976–1992 to the 17 year cold transition of 1959–1975 (Fig. 2c; Table 1), sea level trends reverse signs in most regions of the Pacific Ocean (Fig. 4c, d). Comparing the two 17 year IPO cold transitions of 1959–1975 and 1993–2009, sea level trends show similar patterns and

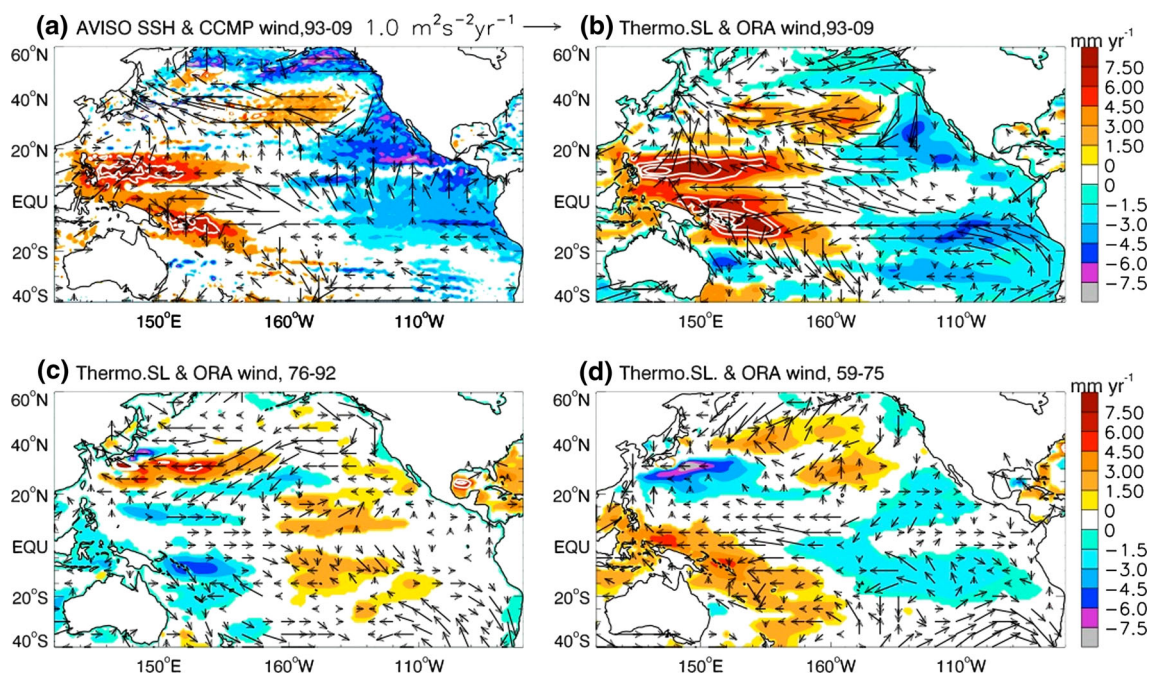


Fig. 4 **a** Linear trend of AVISO multi-satellite SSH (global mean removed) for the 17 year period from 1993 to 2009, which is similar to that of 1993–2010 shown in Fig. 1. This period of time corresponds to IPO cold transition from positive to negative (Fig. 2). Colors show trend values exceeding 95 % significance and white regions show trend values below 95 % significance. The white line contours in the WTP show trend values ≥ 6 mm year⁻¹ with an interval of

1.5 mm year⁻¹. Arrows are linear trends of CCMP pseudo wind stress for the same time period. **b** Same as (a) but from the upper 700 m thermosteric sea level trends and ECMWF ORA-S3 pseudo wind stress; **c** same as (b) but for the 17 year IPO warm transition period from 1976 to 1992; **d** same as (b) but for the 17 year IPO cold transition period from 1959 to 1975. Units: mm year⁻¹ for sea level trends and m²s² year⁻¹ for pseudo wind stress trends

signs in the eastern and northern Pacific, but exhibit marked contrast in the western tropical and subtropical Pacific (Fig. 4b, d). Large-amplitude acceleration of SLR has occurred in the WTP and no sea level fall is detected south of Japan from 1993 to 2009. The sea level increase south of Japan associated with the IPO warm transition from 1976 to 1992 disappears but does not reverse sign from 1993 to 2009, which is in contrast to the strong sea level fall during the IPO cold transition of 1959–1975. In this paper, we will focus on examining tropical Pacific Ocean, and the extra-tropical Pacific sea level variability will be studied in our future research.

The intensified WTP SLR since the early 1990s is also seen in ORA-S3 and reconstructed sea level data (Fig. 5), and the thermosteric sea level agrees the best with the satellite observations for their overlapping periods regarding both spatial pattern and amplitude (compare Figs. 4a, b, 5a, d). The ORA-S3 product generally reproduced the satellite and thermosteric sea level trends, except for the extratropical south Pacific where ORA-S3 significantly overestimated the SLR in the central and western basin (Fig. 5a). The SSHA correlation map between thermosteric sea level and ORA-S3 data from 1959 to 2009 shows good agreements in most regions of the Pacific basin (Fig. 6a),

with correlation coefficients being 0.89, 0.93 and 0.87 in the western tropical north Pacific (WTNP), western tropical south Pacific (WTSP) and central equatorial Pacific (CEQP), respectively (Fig. 6d–f), the key regions of decadal-multidecadal sea level intensification. The reconstructed sea level produced a too strong sea level fall in the eastern equatorial Pacific and too weak SLR in the WTP (Fig. 5d).

While the thermosteric sea level and ORA-S3 data have reasonable agreements, there are apparent differences before the 1970s (Fig. 6d–f), which affects the sea level trend for 1959–1975. For example, in the WTP near 10°N, no variability is detected in thermosteric sea level, whereas there is marked SLR in ORA-S3 data (Figs. 4d, 5c). Causes for the differences are unclear. One possibility is that larger errors in ORA-S3 wind fields for this earlier time period induce errors in sea level. Another speculation is that the lack of salinity effect in thermosteric sea level could contribute to some of the regional differences, even though thermosteric effect dominates total steric sea level in the Indo-Pacific basin during the past few decades (Nidheesh et al. 2012). Paucity of observations in this earlier decade may also cause uncertainties in detecting thermosteric sea level variability. Given these uncertainties, we should

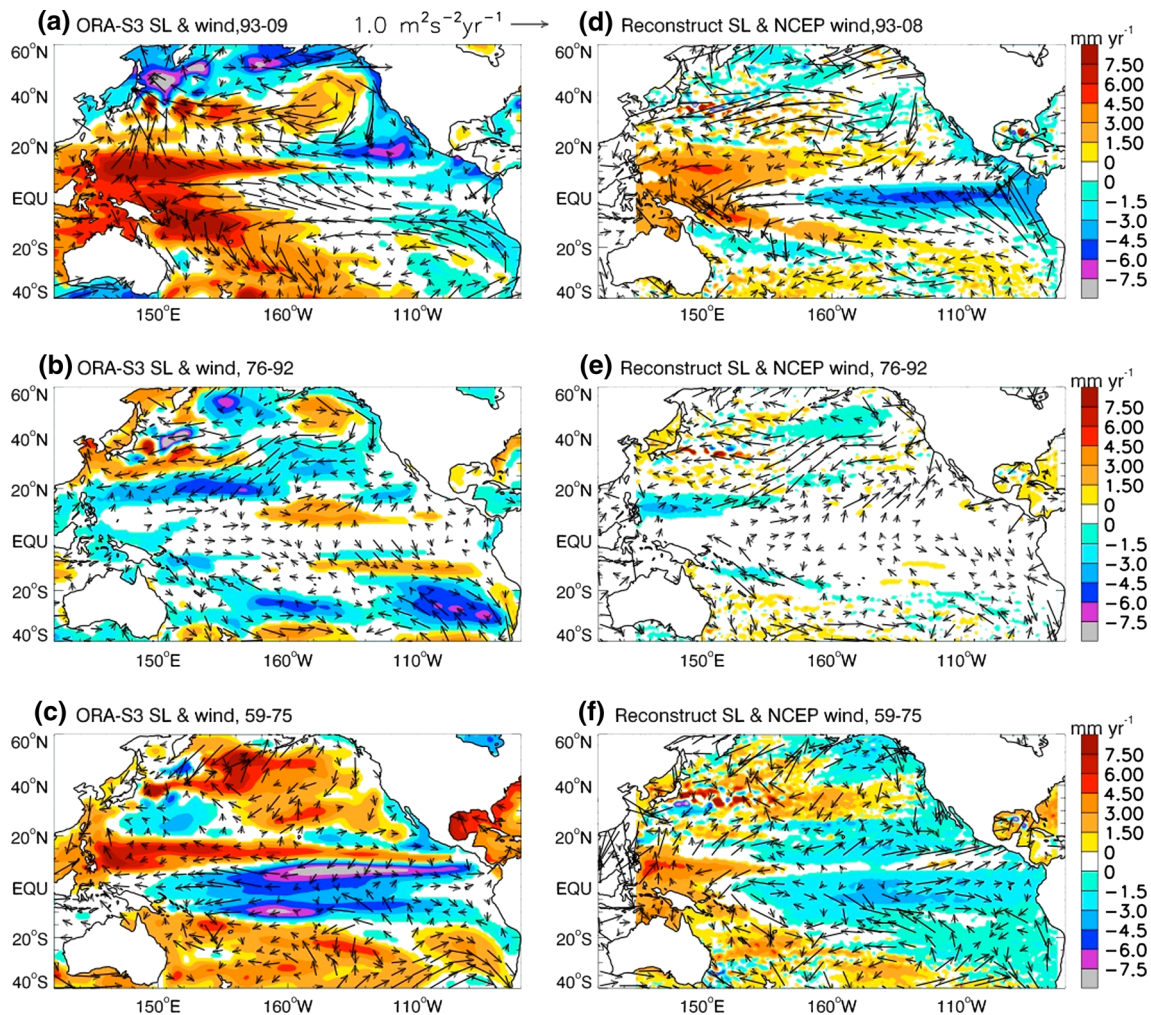


Fig. 5 **a** Linear trend of ECMWF ORA-S3 SSH (global mean removed) for 1993–2009; values exceeding (*below*) 95 % significance are shown in *colors* (*white*); *arrows* are linear trends of ORA-S3 pseudo wind stress for the same time period; **b** Same as (**a**) but for

1976–1992 period; **c** same as (**a**) but for 1959–1975; **d**, **e** and **f** Are the same as (**a**), (**b**), (**c**) but for the Hamlington et al. (2011) reconstructed sea level and NCEP pseudo wind stress. Units: mm year^{-1} for sea level trend and $\text{m}^2\text{s}^{-2}\text{ year}^{-1}$ for pseudo wind stress trends

interpret the sea level and wind signals for the early period with caution. Nevertheless, both datasets exhibit consistent, large-amplitude intensification of SLR in the WTP, and sea level fall in most areas of the eastern and northern Pacific since the early 1990s, as quantified by the sea level trend differences between the two IPO cold transition periods (Fig. 7).

3.2.2 Effects of surface winds

The accelerated WTP SLR since the early 1990s is associated with intensified easterly trade winds relative to the mean in the central and western tropical Pacific basin (arrows in Figs. 4a, b, 8), where the anomalous easterlies are much stronger than those of 1959–1975 (Fig. 4d). Comparing to the satellite-observed CCMP winds, the ORA-S3 products are more faithful than the NCEP winds

in producing the intensified easterlies in the tropics and southerlies near 10–40°N in the central-western Pacific (Figs. 4a, b, 5d), even though both reanalysis products overestimate the southeasterlies in the southeast tropical Pacific. Indeed, the spatial patterns of sea level trends from the LOM forced solely by ORA-S3 surface wind stress (Fig. 9) resemble the overall patterns of ORA-S3 sea level (Figs. 5a–c, 7b), and the LOM reasonably simulates the sea level variability in most region of the tropical Pacific Ocean, as demonstrated by its good agreements with thermosteric sea level and ORA S3 product (Fig. 6b–f). These results demonstrate the deterministic role played by winds in driving the observed, multidecadal sea level variability patterns in the tropical Pacific basin, particularly the recent intensification of WTP SLR. Note that the sea level signals are more spatially confined and have larger amplitudes in the LOM than the ORA-S3 data. The

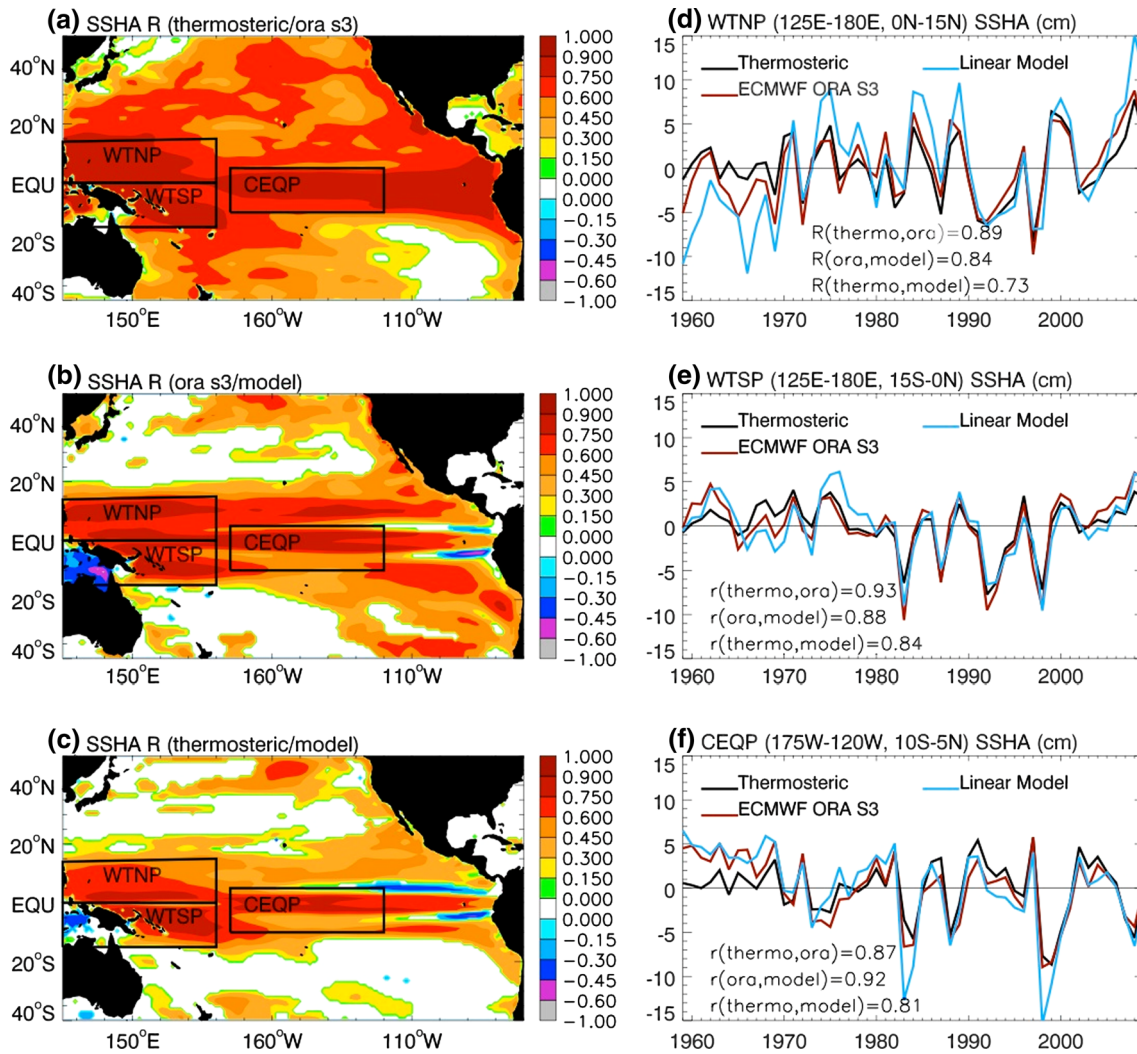


Fig. 6 Correlation maps (>90 % significance) for annual mean SSHAs from 1959 to 2009 (with the mean of 1959–2009 removed) between **a** thermosteric sea level and ORA S3 data, **b** ORA S3 data and linear ocean model (LOM) output, and **c** thermosteric sea level and LOM output. The 3 boxes show WTNP, WTSP and CEQP regions. White areas show correlations below 90 % significance.

d Time series of annual mean SSHAs averaged in the WTNP from thermosteric sea level (black), ERA S3 data (red) and LOM output (blue); their correlation coefficients (>99 % significance) are shown in the panel. **e** and **f** are the same as **(d)** except for the WTSP and CEQP, respectively

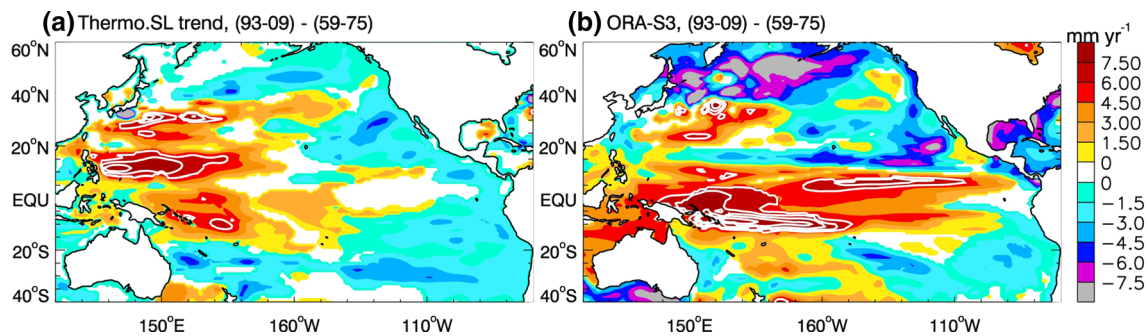


Fig. 7 a Linear trend difference between the two negative IPO transition periods of 1993–2009 and 1959–1975 from the upper-700 m thermosteric sea level (global mean removed). Colored (white) regions show trend values exceeding (below) 95 % significance.

White line contours show trend values $\geq 6 \text{ mm year}^{-1}$, with an interval of 1.5 mm year^{-1} . **b** Same as **(a)** but for ERA-Interim (ORA-S3) reanalysis sea level data

quantitative differences likely result from the lacks of nonlinear advection, variations of stratification, and surface buoyancy flux forcing in the LOM.

3.2.3 Changes in Pacific winds associated with IPO and TIO SST variability

Given that the IPO did not enhance during recent decades (Sect. 3.1) and thus cannot explain the strengthened easterlies that drive the accelerated WTP SLR (Sect. 3.3.2), what are the causes for the intensified surface winds in the WTP? As discussed in Sect. 3.1, on multidecadal timescales, the relationship between IPO and TIO SST has

changed from in phase before 1998 to out of phase thereafter (Fig. 2c). Below, we further examine the time evolution of the Indo-Pacific SST patterns associated with each multidecadal IPO phase period. During the negative IPO phase of 1945–1977, cold SSTAs in the tropical Pacific correspond to cold SSTAs in the TIO (Fig. 10a). From 1978 to 1998, the IPO is positive and the SSTAs reverse, with warm SSTAs in the tropical Pacific corresponding to warm SSTAs in the TIO (Fig. 10b). In contrast, during the 1999–2010 negative IPO phase, cold tropical Pacific corresponds to warm TIO instead of a cold one (Fig. 10c). When the IPO makes its cold transition from 1993 to 1999, the TIO stays warm and does not follow the decreasing IPO index, whereas it does in the preceding decades (red and black lines of Fig. 2c). Comparing the two negative IPO periods of 1945–1977 and 1999–2010, there is a marked difference: Positive SSTAs encompass the entire TIO and western Pacific (west of ~160°E) during 1999–2010, whereas negative SSTAs occupy these regions during 1945–1977 (Fig. 10a, c). The warm TIO from 1999 to 2010 is associated with a steady warming trend since the 1950s (Fig. 2c, red curve). The warming rates are quantified in Fig. 11 for both HadiSST and Hurrell SST, which show faster warming in the equatorial (10°S–10°N) Indian and WTP basins from 1950 to 2010 (Fig. 11a, b), during which the equatorial Indian Ocean warms by ~1 °C or larger, while the central-eastern tropical Pacific and Atlantic warm by ~0.5 °C in most areas.

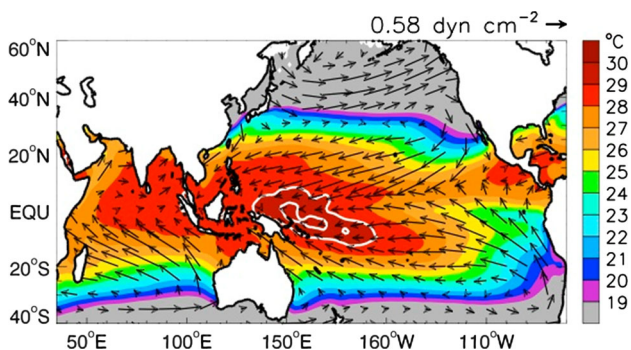


Fig. 8 Mean HadiSST (°C) and ORA-S3 surface wind stress (dyn cm⁻²) for the 1950–2010 period. The white contours are for 29 and 29.4 °C isotherms

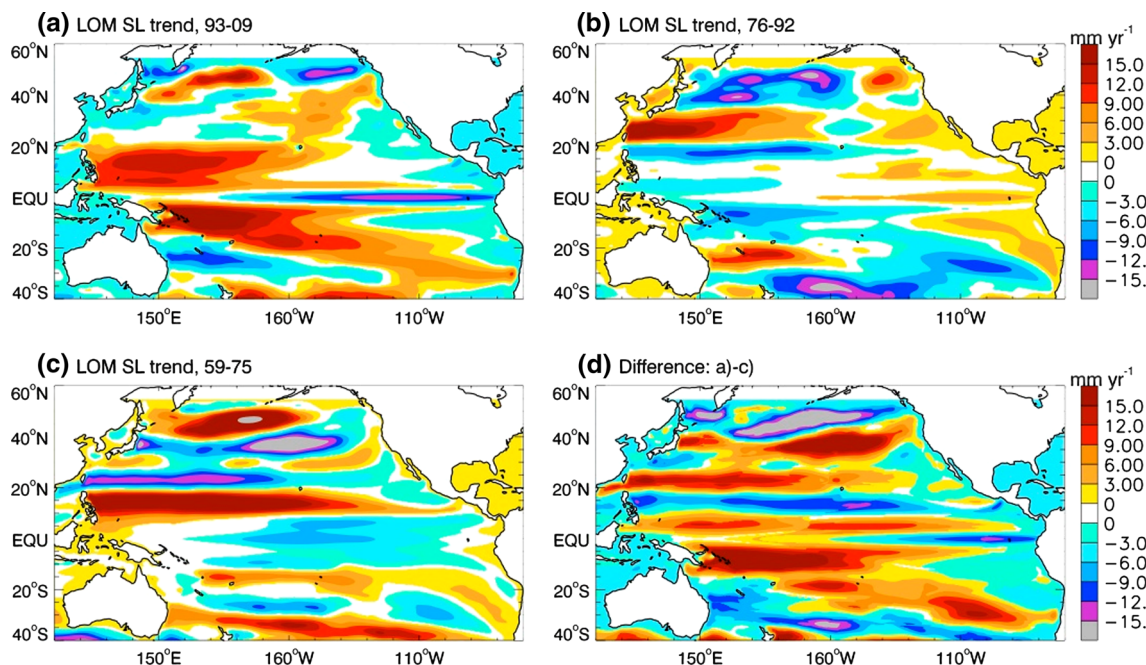


Fig. 9 Linear trend of sea level from the LOM forced by ORA-S3 winds for the period of **a** 1993–2009, **b** 1976–1992, **c** 1959–1975 and **d** the difference between (a) and (c). Colors (white areas) show trend values exceeding (below) 95 % significance. Units: mm year⁻¹

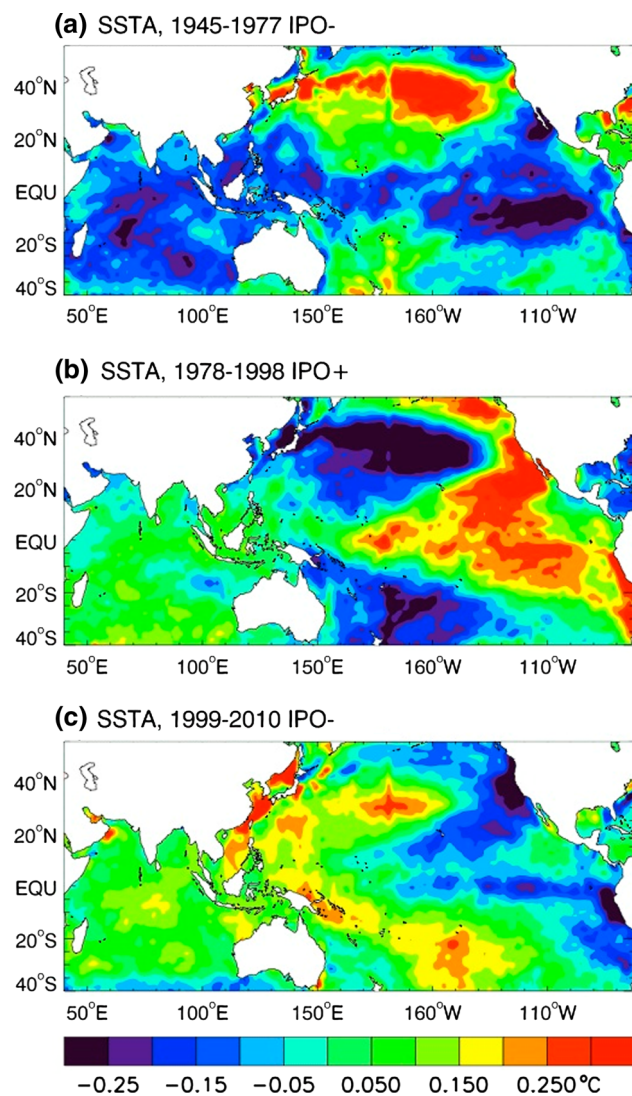


Fig. 10 **a** Indo-Pacific basin SSTA (°C) averaged for the negative IPO period of 1945–1977, based on the unfiltered monthly HadiSST from 1900 to 2010 with the mean seasonal cycle and linear trend from 1900 to 2010 removed; **b** same as (a) but for positive IPO phase from 1978 to 1998; **c** Same as (a) but for negative IPO phase of 1999–2010

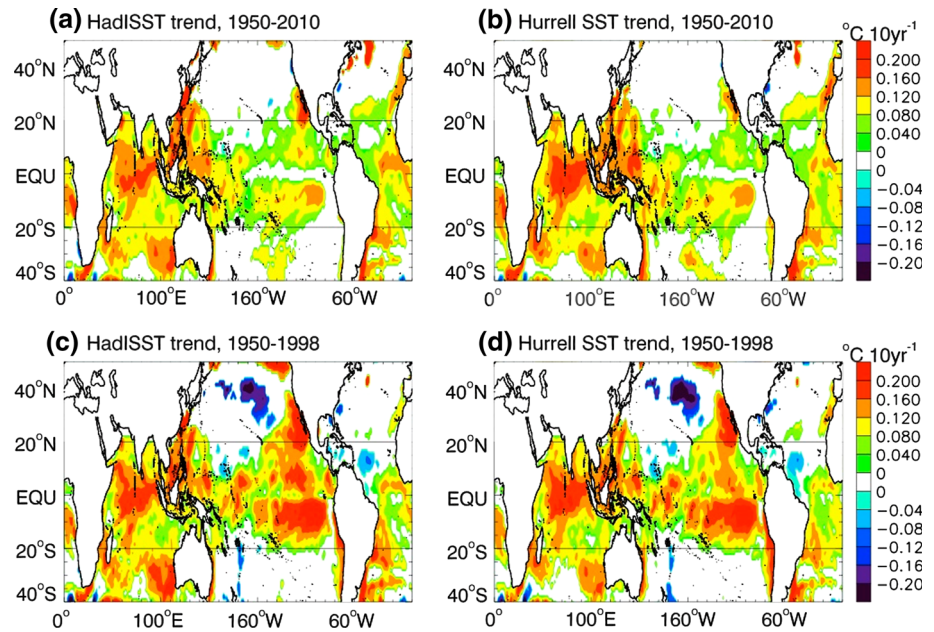
How does the ~ 0.5 °C warmer TIO affect the Pacific wind and sea level? To answer this question, we performed two idealized AGCM experiments, and their difference, AGCM_TIO0.5, isolates the effect of 0.5 °C warmer TIO. These experiments show that the warmer TIO induces surface easterlies and negative Ekman pumping velocity (w_e) in the tropical Pacific, with maximum amplitudes occurring in the western basin west of 160°E (Fig. 12b). These results are consistent with previous studies, which suggest that Indian Ocean tropospheric warming enhances the Pacific Walker Circulation and surface equatorial easterlies in the Pacific via atmospheric bridge during recent decades (Luo et al. 2012), and favors generating La Niña-like state particularly in the western tropical Pacific basin

(Okumura et al. 2011). The anomalous easterlies and negative w_e increase the WTP sea level through both local and remote processes. The enhanced equatorial easterlies and negative w_e in the central and eastern tropical basins generate westward propagating Rossby waves associated with high sea level on both sides of the equator. On decadal and multidecadal timescales, this process is quasi-steady, because Rossby waves propagate fast near the equator. The anomalous winds produced by TIO warming may have played an important role in accelerating the WTP SLR since 1993.

Note that west of $\sim 150^\circ\text{E}$ where anomalous easterlies and negative w_e induced by the TIO warming obtain their maximum amplitudes, satellite observed CCMP winds, ERA-Interim and ECMWF ORA-S3 products show weak or \sim zero wind magnitudes with positive w_e trends in some areas (Fig. 12a, c, d). What likely happened is that the WTP warming (Fig. 10c), which overlies on the high mean SST (>29 °C) and strong SST gradients near 150–160°E in the equatorial region (Fig. 8), causes much stronger convection in the region and along the South Pacific Convergence Zone than in the Maritime continents (Fig. 13). While the enhanced convection near 150°E–160°E enhances equatorial easterlies to the east, it also drives westerlies to the west, thereby producing anomalous westerlies and positive w_e west of 150°E. The westerlies and positive w_e are balanced by the easterlies and negative w_e forced by the warm TIO, and thus producing weak winds in the WTP in the observations (Fig. 12a, c, d). Without the TIO warming, the WTP SLR will be significantly reduced.

Even though the TIO warming might be essential for intensifying the WTP SLR during recent decades, it is the tropical Pacific air–sea interaction that determines the basin-wide surface winds, which drive the basin-wide sea level trend patterns since 1993. To demonstrate this point, we analyze the results from AGCM_GOGA (global monthly SST forcing) and TOGA (tropical SST forcing) experiments. Linear trends of surface wind stress and w_e from 5-member ensemble mean of AGCM_GOGA (Fig. 12e) resemble those of the observed (compare Fig. 12e with a, c, d). There are, however, some quantitative differences. The most apparent difference occurs in the tropical Pacific, where the model produces strong southwesterlies and positive w_e in the western-central basin near 10–20°N, whereas the observations show southerlies and weak negative w_e . The basin-wide wind patterns shown in AGCM_GOGA are successfully simulated by AGCM_TOGA (Fig. 12f), suggesting that tropical air–sea interaction plays a deterministic role in generating the basin-wide surface winds and sea level patterns. Given that the tropical Atlantic SST variability has little effect on SST (Fig. 1 of Sutton and Hodson 2005) and surface winds in the western

Fig. 11 Linear trend of SST ($^{\circ}\text{C year}^{-1}$) for the 1950–2010 period for **a** HadISST; **b** Hurrell SST; linear trend of SST for the 1950–1998 period for **c** HadISST; **d** Hurrell SST. Values that exceed (*below*) 95 % significance are shown in colors (*white*). The two horizontal lines mark the 20°S and 20°N latitudes



and central tropical Pacific basin (Fig. 6 of Kushnir et al. 2010), the observed surface winds result primarily from tropical Indo-Pacific SST forcing. Consequently, the differences between Fig. 12a, b result largely from tropical Pacific SSTAs.

As discussed earlier, in addition to the TIO warming, the 1999–2010 negative IPO phase is associated with WTP warming, whereas the 1945–1977 negative IPO phase is associated with WTP cooling (Fig. 10a, c). The WTP warming enhances east–west SST gradient and western equatorial convection, and therefore strengthens the equatorial easterlies in the central-western equatorial basin. It is unclear, however, whether this SST pattern change is part of the IPO natural variability, or it is affected by anthropogenic warming. The steady Indian Ocean warming trend since the 1950s (Figs. 2c, 11) is attributed to increased greenhouse gases (Du and Xie 2008). As shown in Fig. 2c, however, the TIO cooling from 1945 to 1977 and warming from 1978 to 1998 coincide with the variability of IPO index, with IPO–/IPO+ being associated with TIO cooling/warming. Therefore, it is possible that the IPO warm transition also plays some role in warming up the TIO from the 1950s to 1990s. This speculation is supported by the considerably faster warming rates in the central-eastern tropical Pacific but only slightly faster warming in the TIO from 1950 to 1998 (compare Fig. 11c, d–a, b).

Of particular interest is that while the IPO enters its negative phase after 1998, the TIO stays warm and does not follow the IPO index (Fig. 2c), suggesting that the warm TIO is not likely a response to IPO phase change. Rather, it

is contributed from the steady TIO warming trend that is largely attributed to anthropogenic warming by previous study. This argument is consistent with the somewhat slower TIO (and WTP) warming rates from 1950 to 2010 than those for 1950–1998, but markedly reduced warming in the tropical Pacific (Fig. 11). Consequently, it is possible that anthropogenic warming plays some role in causing the changing IPO/TIO SST relationship on multidecadal timescales. Cross-spectral analysis shows that on multidecadal timescales, coherency between the TIO and WTP SSTA is high (>0.7), and the TIO SSTA leads that of the WTP (not shown). The coherency is significantly lower with the CEQP SSTA. Meyssignac et al. (2012) attributed the 1993–2009 sea level dipole pattern in the tropical Pacific to natural variability, because similar patterns are found in climate model control simulations without anthropogenic forcing. Our results suggest that natural internal variability associated with the IPO cold transition determines the basin-scale sea level trend pattern since 1993. Warming in the WTP and TIO, however, are essential for causing the intensification of the WTP SLR, and the TIO warming may have been contributed partly from anthropogenic forcing. This regional intensification, rather than basin-wide pattern alterations, requires particular attentions when we assess the relative roles of IPO natural variability and anthropogenic forcing. The evidence provided in this paper supports, but is not sufficient to prove, the anthropogenic warming effect. Attributing the anthropogenic effect versus natural variability is beyond the scope of this study, but it is an essential next step for our future research.

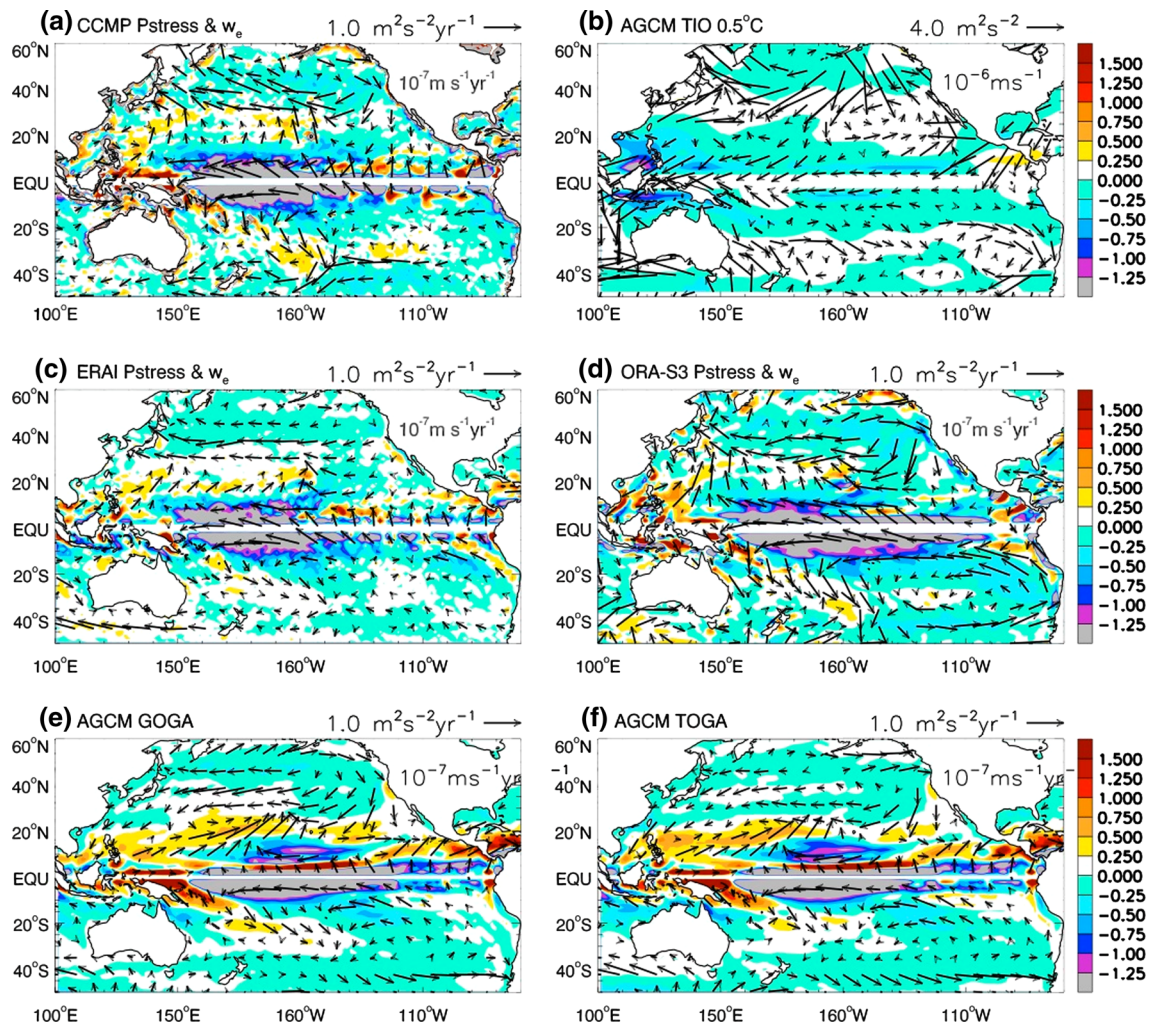


Fig. 12 **a** Linear trend of CCMP surface pseudo wind stress (arrows; $m^2s^{-2}yr^{-1}$) and Ekman pumping velocity w_e (color contours; $10^{-7}ms^{-1}yr^{-1}$) from 1993 to 2009, where $w_e = \frac{\partial}{\partial x}(\frac{\tau^y}{\rho_0 f}) - \frac{\partial}{\partial y}(\frac{\tau^x}{\rho_0 f})$, ρ_0 —water density, f —Coriolis parameter, (τ^x, τ^y) —(zonal, meridional) wind stress; **b** Surface pseudo wind stress and w_e from 45

member ensemble mean of AGCM_TIO0.5 idealized experiment; **c**, **d** are the same as **(a)** but for ERA-Interim and ECMWF ORA-S3 winds from 1993 to 2009; **e** same as **(a)** except for 5-member ensemble mean of AGCM_GOGA experiment for 1993–2008; **f** Same as **(e)** but for AGCM_TOGA from 1993 to 2008

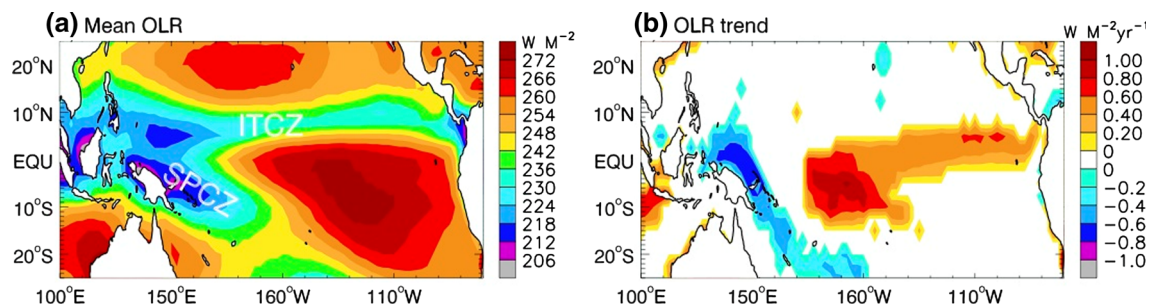


Fig. 13 **a** Mean Outgoing Longwave Radiation (OLR; $w m^{-2}$), which represents tropical deep convection, for the 1993–2009 period in the tropical Pacific Ocean; the Intertropical Convergence Zone

(ITCZ) and South Pacific Convergence Zone (SPCZ) are labeled; **b** Linear trend of OLR ($w m^{-2} yr^{-1}$) for 1993–2009. Values that exceed (below) 95 % significance are shown in colors (white)

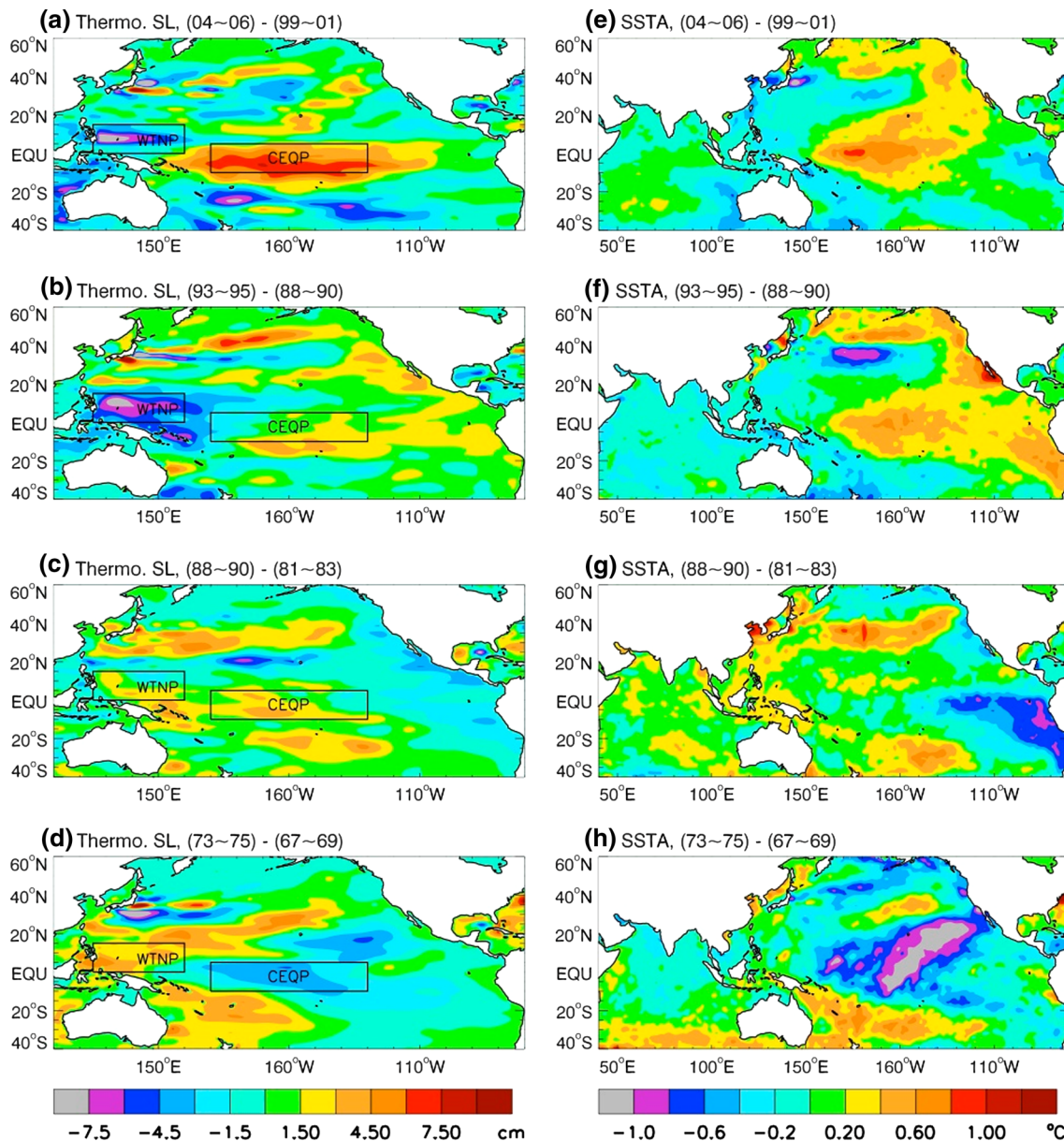


Fig. 14 **a** Sea level difference between high IPO index years (2004–2006 average) and low IPO index years (1999–2001 average) for the Pacific Ocean, which measures the amplitude and spatial pattern of decadal sea level variability corresponding to the 10–20 year IPO variability within the 1999-present multidecadal IPO+ phase (Fig. 2c), based on the 8 year lowpassed upper-700 m thermometric sea level data (global mean removed). The two boxes are the regions used in Fig. 16; Table 2. **b, c** Are the same as (a) except

for the differences between high and low IPO index years for (1993–1995)–(1988–1990), and between IPO low and high years for (1988–1990)–(1981–1983), which are within the 1977–1998 multidecadal IPO+ phase. **d** Same as (a) but for (1973–1975)–(1967–1969) within the multidecadal IPO– phase of 1945–1977. **e–h** Are the same as (a–d), respectively, except for 8 year lowpassed HadiSST (with mean and linear trend for 1870–2012 removed before the filtering) for the Indo-Pacific basin

3.3 Decadal sea level variability and amplification since late 1980s or early 1990s

3.3.1 Western tropical Pacific region

The IPO index varies on 10–20 year timescales within each of the IPO multidecadal phase period (Fig. 2c). While there is no apparent intensification of 10–20 year IPO amplitudes

since the late 1980s comparing to the preceding decades (Sect. 3.1), the corresponding sea level variability amplifies considerably in the WTP (compare Figs. 14a, d, 15c, e, f, h, 16e; Table 2). The large-amplitude 10–20 year sea level signals enter the TIO via the Indonesian Throughflow region and exert stronger influence on the TIO than previous decades (Fig. 15). Note that to assess the spatial patterns and amplitudes of sea level variability associated

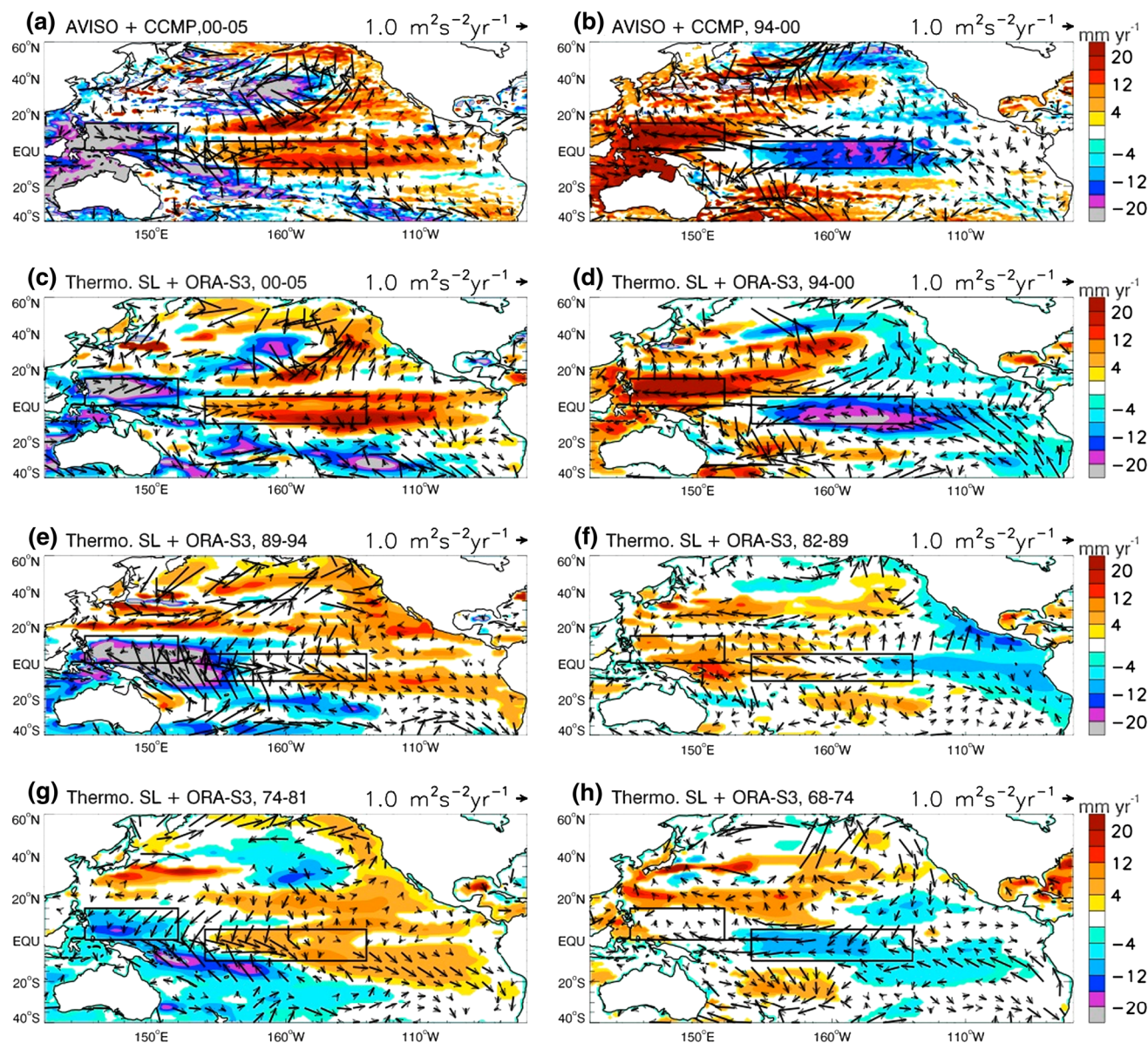


Fig. 15 **a** Linear trend of satellite observed SSH with global mean removed (mm yr^{-1}); *color contours* show trend values $>90\%$ significance) and CCMP pseudo wind stress (*arrows*; $\text{m}^2\text{s}^{-2}\text{yr}^{-1}$) from 2000 to 2005, when IPO varies from cold to warm on 10–20 year timescales (see Fig. 2c for IPO index); **b** same as (a) but for 1994–2000 IPO cold transition; **c** and **d** are the same as (a) and

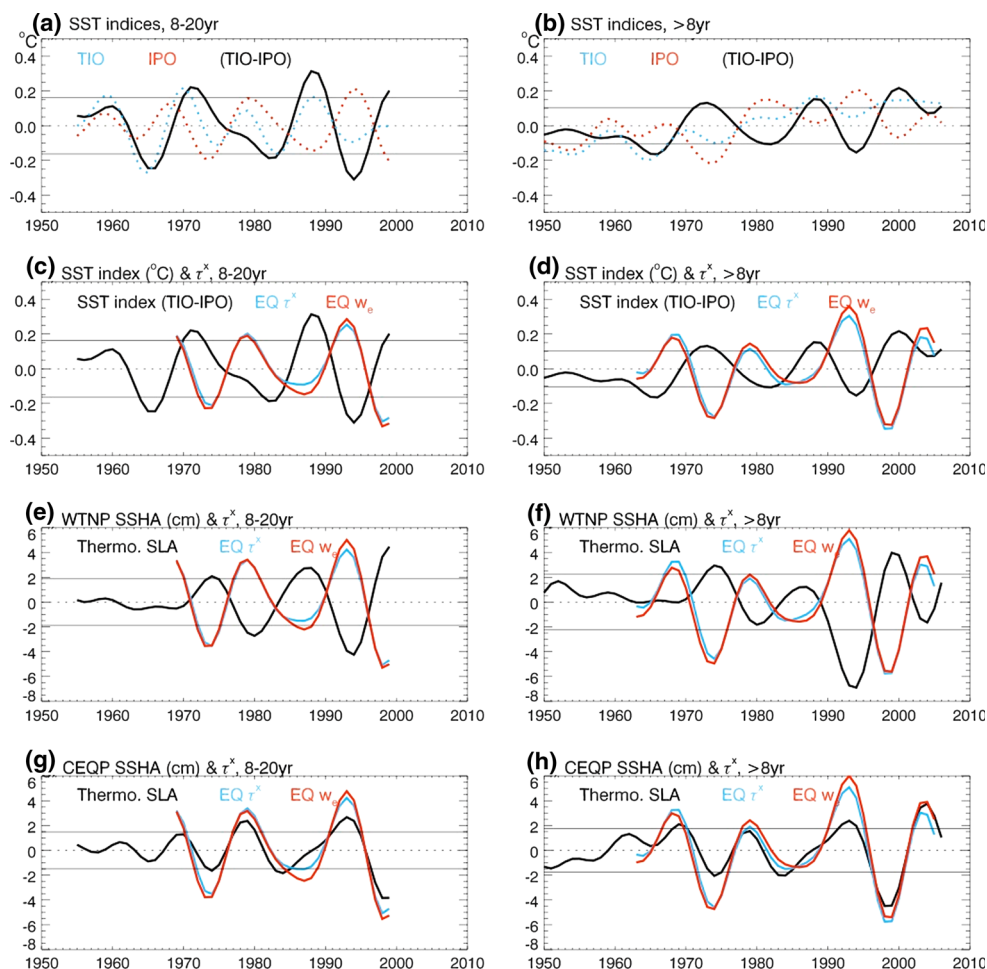
(b), except for the upper-700 m thermosteric sea level and ORA-S3 pseudo wind stress; **e** and **g** in the *left column* are the same as (c) except for IPO index changing from low to high for 1989–1994 and 1974–1981; **f** and **h** in the *right column* are the same as **d** except for IPO index varying from high to low during 1982–1989 and 1968–1974. The *two boxes* mark the same regions as those in Fig. 14

with the 10–20 year IPO, we take the 8 year lowpassed sea level differences between the IPO index high and low years within each IPO multidecadal phase period (Fig. 14a–d). This method avoids aliasing the effect of IPO multidecadal phase transitions. The linear trend of sea level that corresponds to each time period of Fig. 14a–d is shown in Fig. 15c, e, f and h, respectively.

The intensification of decadal sea level since the early 1990s is particularly strong in the WTNP (western box of Fig. 14), with a STD of 10–20 year sea level variability

being 2.84 cm from 1991 to 2005, comparing to 1.12 cm for 1963–1976 and 1.31 cm for 1977–1990, based on the 8 year lowpassed thermosteric sea level data (Table 2; Fig. 16e). The 10–20 year sea level variability averaged in the WTNP region exceeds 1 STD near 1988 and 2 STDs near 1993 (Fig. 16e, black curve), whereas before 1988 it is near or within 1 STD. Note that near 1980, negative sea level anomaly also exceeds 1 STD. The variability amplitude from 1980 to 1988, however, is notably larger than that from 1974 to 1980. The intensification of 10–20 year

Fig. 16 **a** Time series of 8–20 year bandpassed IPO index (red dotted), TIO SST PC1 (blue dotted) and their difference (TIO–IPO; black solid) from 1955 to 1999, the same period as for the 8–20 year thermosteric sea level below; to exclude the filter's end point effect, 10 years data from each end are excluded; **b** Same as (a) except for 8 year lowpassed values for 1950–2005; **c** 8–20 year (TIO–IPO) SST index (black), zonal wind stress τ^x (scaled up by 3 dyn cm^{-2}) averaged over (140°E – 170°E , 5°S – 5°N) and Ekman pumping velocity w_e (scaled up by $2 \times 10^5 \text{ m s}^{-1}$) averaged over (140°E – 170°E , 10°S – 10°N); calculations over 130°E – 180°E longitudes provide similar results; **d** Same as (c) except for 8 year lowpassed values; **e** and **f** are the same as (c) and (d), except for upper-700 m thermosteric sea level in the WTNP, τ^x (scaled by 50 dyn cm^{-2}) and w_e (scaled by $1/3 \times 10^7 \text{ m s}^{-1}$); **g** and **h** are the same as (e) and (f) except for the thermosteric sea level in the CEQP



sea level variability of WTP is also detected by ORA-S3 product (Table 2), and can be visually identified in tide gauge observations at stations Malakal and Guam, which are located in the western tropical north Pacific (Fig. 5 of Merrifield 2011) where the 10–20 year sea level variability obtains large amplitudes since the late 1980s especially since the early 1990s (Figs. 14, 15, 16).

Why does the 10–20 year sea level variability in the WTP amplify, whereas the 10–20 year IPO index does not? To answer this question, we examine the Indo-Pacific SST variability particularly in the tropics, where air–sea interaction is shown to determine the basin-wide surface winds that drive the basin-wide multidecadal sea level patterns (Sect. 3.2.3). Within the 1945–1977 multidecadal IPO–phase, IPO index goes from high to low from 1968 to 1974 (Figs. 2c, 16a). The 8 year lowpassed SST difference between 1974 and 1968 shows negative IPO pattern in the Pacific, which corresponds to large-scale cooling in the TIO (Figs. 2c, 14h, 16a). This Indo-Pacific SSTA combination resembles the effect of La Niña on interannual timescales, which induces basin-wide cooling in the TIO.

Our idealized AGCM experiment shows that TIO cooling induces anomalous westerlies in the WTP and along the equator (opposite pattern of Fig. 12b; Sect. 2.3), which act to reduce the WTP sea level and thus counteract the WTP SLR caused by the anomalous easterlies associated with the negative IPO (Figs. 14d, 15h).

Within the 1978–1998 multidecadal IPO+ period, IPO index changes from high to low during 1982–1989 (Figs. 2c, 16a), warm SSTA appears in the TIO and central-western tropical Pacific, and cold SSTA occurs in the eastern south Pacific (Fig. 14g). This SSTA pattern is a transition from the Indian-Pacific SSTA in phase relation (Fig. 14h) to out of phase relation (Fig. 14f). This relation change occurs near 1985, after which decadal TIO warming/cooling corresponds to Pacific cooling/warming (Figs. 2c, 16a), as discussed in Sect. 3.1. From 1989 to 1994, IPO varies from cold to warm, and the TIO changes from warm to cold (Figs. 14f, 16a). The cold TIO acts in concert with the warm Pacific, which is represented by the amplified (TIO–IPO) difference index in late 1980s (Fig. 16a, c, black curve), producing westerly wind anomalies and positive w_e in the tropical Pacific

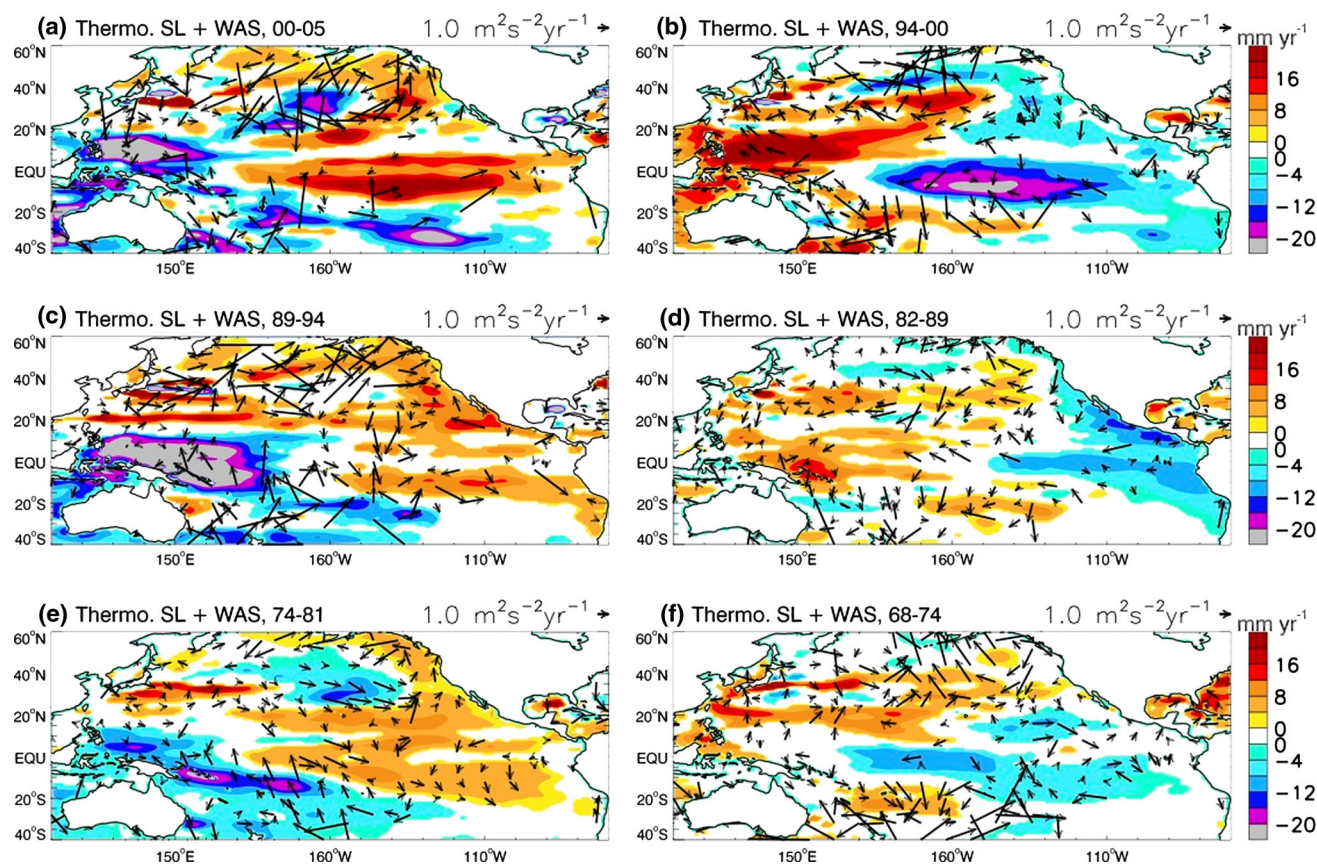


Fig. 17 Linear trend of upper-700 m thermosteric sea level with global mean removed (color contours; mm year^{-1}) and pseudo wind stress (arrows; $\text{m}^2\text{s}^{-2}\text{year}^{-1}$) from Wave- and Anemometer-Based Sea Surface Wind (WASWind) during the six periods shown in Fig. 15c, h

(Fig. 16c, blue and red curves), and therefore causes large amplitude sea level fall in the WTP (Figs. 14b, 15e, 16e).

Within the 1999–2010 multidecadal IPO– phase, IPO index varies from low near 2000 to high near 2005. The IPO variability, however, is weak relative to the previous 10–20 year variability amplitudes (Figs. 2c, 16b). Meanwhile, the TIO SST cools in most areas (e.g., the Arabian Sea, Bay of Bengal and southeast Indian Ocean), even though it warms in a region near the equator (Fig. 14e). This equatorial warming might be a response to the warm tropical Pacific via atmospheric bridge, as discussed earlier. Note that the tropical Pacific warming obtains the maximum near the central equatorial Pacific, with larger amplitudes than that from 1989 to 1994 (Fig. 14f). With this SST combination, sea level reduces rather rapidly in the WTP, with a reduction area much smaller than that from 1989 to 1994, a period when TIO exhibits basin-wide cooling (Figs. 14a, b, 15c, e). Different from the 1989 to 1994 case, sea level shows fast rise in the central-eastern equatorial basin from 2000 to 2005, whereas that for 1989–1994 is very weak (Figs. 15c and 14a versus 15e and 14b). This central equatorial Pacific decadal sea level variability will be discussed next (Sect. 3.3.2). Note that the 10–20 year data from 2000 onward are excluded in

Fig. 16 (left column) by removing the filter's end point effect. The larger variation of (TIO–IPO) difference than IPO index is seen in 8 year lowpassed data (Fig. 16b), and the amplified wind and SSHA responses can be identified in Fig. 16d, f. Given that surface wind anomalies converge to the central equatorial region where warm SSTA is large (Figs. 14e, 15a, c) and mean SST gradient is strong (mean SST $>28^\circ\text{C}$; Fig. 8), the stronger SSTA in the central-equatorial basin may have also contributed to the strong anomalous westerlies and thus the rapid WTP sea level fall.

The intensification of easterly wind anomalies in the WTP region from 1994 to 2000 is also shown in WASWind data, comparing to other periods when IPO index varies from high to low (right panels of Fig. 17), and to the anomalous westerly wind magnitude from 1974 to 1981 when IPO transits from negative to positive (Fig. 17e), even though the wind trend patterns are not continuous due to missing data.

3.3.2 Central-equatorial basin and relation to the WTP

By examining the decadal sea level variability patterns within each of the IPO multidecadal period, we see

intensified amplitude in the central equatorial Pacific at the beginning of the twenty-first century (compare Fig. 14a with b–d, Fig. 15c with e, f, h). If we also examine the 1994–2000 period during which IPO index varies from positive to negative, which is decadal scale variability overlying on the multidecadal phase transition (compare Fig. 16a, b, red curves), we find that the 10–20 year timescale sea level fall in the central equatorial basin and the SLR in the WTP appear to be linked (Figs. 15b, d, 16e, g). Both are associated with wind anomalies in the central-western equatorial Pacific (Fig. 16e, g), which in turn are associated with tropical Pacific cooling and TIO warming (Fig. 16a, b). The correlation between WTP and CEQP 8 year lowpassed thermosteric sea level is -0.56 from 1950 to 2006. While strong WTP sea level fall (rise) occurs during 1989–1994 (1994–2000), large amplitude sea level variability in the CEQP primarily appears during 1994–2000 (Figs. 15d, e, 16e, g). This indicates that it is the pattern change of the tropical Pacific SSTA, which shifts to the central Pacific El Niño pattern—with maximum warming occurring in the central equatorial ocean and cooling in the eastern and western equatorial basins (Fig. 14e; the pattern for 1994–2000 is similar)—that may have played a critical role in causing the large amplitude decadal sea level variability in the central-equatorial basin. This structure is in contrast to the multidecadal sea level trend patterns (Figs. 1, 4a), which have large amplitudes in the WTP and eastern basin, with little sea level change in between.

From 1974 to 1981, when IPO decadal scale variability overlies on multidecadal phase transition from negative to positive, the TIO SST increases with the IPO index. This in-phase SSTA between the Indian and tropical Pacific produces a weaker (TIO–IPO) variation and an out of phase effect on surface wind and sea level, and therefore produces weaker wind and sea level variability in the tropical Pacific Ocean than the 1994–2000 period (Figs. 15d, g, 16). The 8 year lowpassed sea level variability, which includes both decadal and multidecadal variability, exceeds 1 STD near 1991 in both the WTP and CEQP region (Fig. 16f, h), and the 8–20 year sea level anomaly in the WTP exceeds 1 STD near 1988 (Fig. 16e). These results explain the increased sea level energy at 8–16 year periods since the late 1980s at the Fremantle tide gauge station (Feng et al. 2010), and the larger Pacific influence on the TIO decadal sea level variability since the early 1990s (Trenary and Han 2013). Note that the intensification of decadal sea level variability in the CEQP is not apparent in ORA-S3 sea level product (Table 2). This intensification, however, is shown in both thermosteric sea level and satellite observed AVISO sea level data, and the two have good agreements (Fig. 15a, d).

3.3.3 The changing role of the Indian Ocean

The WTP sea level variability is significantly correlated with the IPO index, with a correlation coefficient of -0.72 for the 8 year lowpassed sea level and IPO index during 1950–2006 (Table 3). It is, however, essentially uncorrelated with the TIO SST PC1 for the entire 1950–2006 period. This low correlation is because of the correlation coefficient changing sign before and after 1985. The correlation between WTP sea level variability and TIO SST PC1 is negative ($r = -0.48$) from 1950 to 1984, but becomes positive and increased to 0.76 for 1985–2006 (Table 3). These results indicate that decadal variability of TIO SST has played a larger role in determining the WTP decadal sea level change since 1985 than the preceding decades. The 10–20 year TIO SST variability may have resulted from the IPO influence before 1985, with warm/cold tropical Pacific corresponding to warm/cold TIO; however, it is not likely due to the IPO after 1985 since the variability is in opposite sign with the IPO effects obtained by previous studies. Note that the IPO is highly correlated with the 8 year lowpassed ENSO index, and WTP sea level variability has higher correlation with Nino3.4 SST ($r = -0.87$) than with the IPO (Table 3). The correlation between IPO index and TIO PC1 is 0.75 for 1900–1984 and -0.85 for 1985–2008, with both exceeding 99 % significance. To confirm these results, we also analyzed Hurrell SST and Kaplan SST, and obtain similar results on IPO and Indian Ocean SST patterns, their temporal variability (PC1), and the changing correlations between their PC1 s. These results suggest that tropical air–sea interaction over the Indo-Pacific basin may have played a deterministic role in causing the WTP decadal and multi-decadal sea level variability since the 1950s, with the TIO being more active after 1985, and air–sea coupling in the tropical Pacific associated with the IPO is crucial for generating the basin-wide surface winds that drive the basin-wide sea level patterns.

4 Summary and discussions

In this paper, we investigate the changing patterns of Pacific sea level variability on decadal (10–20 year) and multidecadal (>20 year) timescales since the 1950s, and understand their causes. Satellite observations, in situ datasets, reconstructed sea level and ocean–atmosphere reanalysis products (Sect. 2.1) are analyzed to detect the sea level pattern changes. Standalone ocean and atmosphere model experiments are performed to understand the causes.

Our results show that during the decadal and multi-decadal phase transition periods of the IPO, there are basin-

wide changes in surface winds, which are associated with basin-wide changes in sea level. The satellite-observed rapid SLR (global mean removed) in the WTP and fall in the eastern basin from 1993 to 2010, together with the corresponding surface winds (Figs. 1, 4a), are associated with IPO multidecadal phase transition from positive to negative (Fig. 2). The IPO index, however, has not intensified on either decadal or multidecadal timescales since 1993 relative to the preceding decades, while marked intensification of sea level variability is detected on both timescales in the WTP region, and on decadal scale in the central-equatorial basin (Tables 1, 2). The intensified sea level and surface wind signals are robust to cross-dataset differences (Figs. 4, 5, 6, 7, 14, 15, 16, 17; Tables 1, 2). In contrast to the multidecadal sea level trend patterns since 1993, which show a strong west-east dipole with little variability in the central basin (Figs. 1, 4), decadal sea level variability since the early 1990s exhibits a strong WTP versus central-equatorial dipole (Fig. 15a–d). While the 10–20 year thermosteric sea level averaged in the WTP exceeds 1 STD near 1988, the 8 year lowpassed sea level signals (including both decadal and multidecadal variability) exceed 1 STD near 1991 in both WTP and CEQP (Fig. 16).

On multidecadal timescales, the basin-wide sea level patterns—including the intensified WTP SLR since 1993—result primarily from surface wind forcing, as shown by the wind-driven linear ocean model experiment (Figs. 6, 9). The observed basin-wide surface winds—including the intensified easterlies and negative Ekman pumping velocity since the early 1990s (Fig. 16)—result primarily from tropical SST forcing, as shown by the high correlation between wind and (TIO–IPO) index (Fig. 16) and demonstrated by AGCM_GOGA and AGCM_TOGA experiments (Fig. 12). These results suggest that tropical air–sea interaction—particularly in the tropical Indo-Pacific basin—may have played a deterministic role in causing the basin-wide winds and thus sea level patterns in the past few decades.

During the two negative IPO multidecadal phase periods of 1945–1977 and 1999–2010, the major SST difference over the tropical Indo-Pacific basin is warming over the Indian and WTP (west of 150°E) for the latter but cooling for the former period (Fig. 10). The TIO and WTP warm up faster than the rest of the tropical oceans from 1950 to 2010 (Fig. 11). This faster warming explains the SSTA pattern change shown in Fig. 10. Our idealized AGCM experiments show that a warmer TIO generates easterlies and negative Ekman pumping velocity in the tropical Pacific, with largest amplitudes occurring in the WTP basin (Fig. 12b). These wind anomalies act in concert with the anomalous easterlies associated with the IPO cold transition, intensify the zonal winds and Ekman pumping

velocity in the western-central tropical Pacific and drive the accelerated WTP SLR from 1993 to 2010 through both local and remote processes (Sect. 3.2.3; Fig. 16). In addition, the warmer WTP increases the east–west SST gradient and enhances convection in the western equatorial basin (Figs. 8, 10, 13), and thereby strengthening equatorial easterlies and contributing to the rapid WTP SLR. In contrast, during previous decades, the TIO and WTP SSTAs are in phase with the central-eastern tropical Pacific SSTA associated with the IPO (Fig. 16b). This in-phase SSTA relation produces out of phase effects on the WTP SLR and results in weak sea level variability in the WTP region (Fig. 16).

On decadal timescales, the IPO is also associated with basin-wide sea level changing patterns, with rapid WTP SLR corresponding to IPO cold transition (index from high to low), which is analogous to the multidecadal variability (Figs. 14, 15, 16). This intensification of WTP sea level variability is associated with the out of phase relationship between the IPO and TIO SSTA since 1985, with positive (negative) IPO corresponding to cold (warm) TIO (Figs. 2c, 16a; Table 3). This SSTA combination produces “in phase” effects on tropical Pacific wind and sea level variability, because TIO warming (cooling) strengthens the anomalous easterlies (westerlies) and negative (positive) Ekman pumping velocity associated with the negative (positive) IPO (Figs. 14, 15, 16, 17; Sect. 3.3). Before 1985, the situation is opposite, with the TIO SSTA coinciding with the decadal variability of IPO index, which resembles ENSO influence on TIO SST at interannual timescales. This in-phase SSTA patterns produce out of phase effects on surface winds and decadal sea level variability, and thus weaken the WTP sea level amplitude. In contrast, the intensified sea level amplitude in the CEQP (Figs. 15, 16) is likely linked to the shifting pattern of Pacific SSTA to the central Pacific ENSO type (Fig. 14; Sect. 3.3.2).

Previous studies have attributed the steady Indian Ocean warming since the 1950s to anthropogenic greenhouse gases (e.g., Du and Xie 2008). It is likely that the IPO warm transition also has some contributions to the TIO warming trend from 1950 to 1998, given that the TIO SSTA coincides with the multidecadal variability of IPO index from the 1950s to 1990s. After 1998, the IPO enters negative phase, whereas the TIO stays warm and does not follow the IPO index (Fig. 2c), and the warm TIO is contributed from its “persistent warming trend” (Fig. 11) that is attributed to anthropogenic warming. These results indicate that anthropogenic warming may have contributed to the TIO warming and therefore WTP rapid SLR during recent decades. Meyssignac et al. (2012) attributed the fast WTP SLR to natural variability, since similar east–west dipole patterns in the tropical Pacific were found in the simulations of

climate models with and without anthropogenic forcing. Our results show that while the Pacific decadal climate modes are associated with basin-wide sea level patterns, a result consistent with Meyssignac et al. (2012), the “acceleration” of SLR in the WTP region since the early 1990s is likely contributed partly from anthropogenic warming. This inference is supported, but is not proved, by the evidence provided in this paper. It is unclear whether the global climate models are able to simulate such a regional feature, and if yes whether or not this can be detected as a significant pattern change. This raises challenge for climate models for improving their ability to simulate regional SLR, in order to provide meaningful decadal predictions and future projections on regional scales.

Why is the TIO decadal SST variability in phase with the IPO before 1985, but out of phase since 1985? This out of phase relationship may indicate the active role of the TIO in affecting the Indo-Pacific climate, because a warm TIO favors generating a negative IPO pattern. It is clear that the TIO has played a more active role in affecting the Pacific decadal variability since the early 1990s. One hypothesis is that the accelerated warming over the TIO and WTP, where the mean SST is high (Fig. 8), makes convection more sensitive to its SST variability due to nonlinear dependent of convection on SST as the mean SST exceeds the threshold of 27–28 °C (Gadgil et al. 1984; Graham and Barnett 1987; Waliser et al. 1993). The threshold, however, may increase with the increase of tropical SST (Johnson and Xie 2010). A key issue following this study emerges: How is the decadal SST variability generated over the TIO? Note that on interannual timescales, strong ENSO variability still dominates TIO SST both before and after 1985 (Fig. 3). Finally, our analyses are based on relatively short data record. Longer-term, reliable data need to be collected to obtain more statistically significant conclusions.

Acknowledgments We thank Dr. Clara Deser for reading the earlier version of this manuscript and providing helpful comments, and Dr. Adam Phillips for providing the CAM3 TOGA experiment results. Appreciation also goes to Dr. Martin Hoerling for the NSIPP model experiments, and Dr. James McWilliams for stimulating discussions at the earlier stage of this work. W.H. is supported by NSF CAREER award OCE 0847605. Portions of this study were supported by the Office of Science (BER), US Department of Energy, Cooperative Agreement No. DE-FC02-97ER62402, and the National Science Foundation. NCAR is sponsored by the National Science Foundation. D.Y. is supported by China 973 project. We thank NCAR CISL for computational support.

References

- Alexander MA (2010) Extratropical air–sea interaction, SST variability and the Pacific decadal oscillation (PDO). In: Sun D, Bryan F (eds) *Climate dynamics: why does climate vary*. AGU Monograph #189, Washington, DC, pp 123–148
- Alexander MA, Blade I, Newman M, Lanzante JR, Lau NC, Scott JD (2002) The atmospheric bridge: the influence of ENSO teleconnections on air–sea interaction over the global oceans. *J Clim* 15:2205–2231
- Atlas R, Ardizzone J, Hoffman RN (2008) Application of satellite surface wind data to ocean wind analysis. In: *Proceedings of SPIE*, vol 7087, 70870B. doi:10.1117/12.795371
- Balmaseda MA, Vidard A, Anderson DL (2008) The ECMWF ocean analysis system: ORA-S3. *Mon Wea Rev* 136:3018–3034
- Becker M, Meyssignac B, Letetrel C, Llovel W, Cazenave A, Delcroix T (2012) Sea level variations at tropical Pacific islands since 1950. *Global Planet. Change* 80–81:85–98. doi:10.1016/j.gloplacha.2011.09.004
- Bindoff NL, Willebrand J, Artale V, Cazenave A, Gregory J et al (2007) Observations: oceanic climate change and sea level, ch5. In: Solomon S, Qin D, Manning M et al (eds) *Climate change 2007: the physical science basis, contribution of working group I to the fourth assessment report of the intergovernmental panel on climate change*. Cambridge University Press, Cambridge, pp 385–432
- Carton JA, Giese BS, Grodsky SA (2005) Sea level rise and the warming of the oceans in the Simple Ocean Data Assimilation (SODA) ocean reanalysis. *J Geophys Res* 110:C09006. doi:10.1029/2004JC002817
- Cazenave A, Llovel W (2010) Contemporary sea level rise. *Annu Rev Mar Sci* 2:145–173
- Church JA, Gregory JM, White NJ, Platten SM, Mitrovica JX (2011) Understanding and projecting sea level change. *Oceanography* 24(2):130–143
- Collins WD et al (2006) The community climate system model version 3 (CCSM3). *J Clim* 70:2122–2143
- Copsey D, Sutton R, Knight JR (2006) Recent trends in sea level pressure in the Indian Ocean region. *Geophys Res Lett* 33:L19712. doi:10.1029/2006GL027175
- Dai A (2012) The influence of the inter-decadal Pacific oscillation on US precipitation during 1923–2010. *Clim Dyn*. doi:10.1007/s00382-012-1446-5
- Deser C, Phillips AS (2006) Simulation of the 1976/1977 climate transition over the North Pacific: sensitivity to tropical forcing. *J Clim* 19:6170–6180
- Deser C, Phillips AS (2009) Atmospheric circulation trends, 1950–2000: the relative roles of sea surface temperature forcing and direct atmospheric radiative forcing. *J Clim* 22:396–413. doi:10.1175/2008JCLI2453.1
- Deser C, Phillips AS, Hurrell JW (2004) Pacific interdecadal climate variability: linkages between the tropics and North Pacific during boreal winter since 1900. *J Clim* 17:3109–3124
- Deser C, Capotondi A, Saravanan R, Phillips AS (2006) Tropical Pacific and Atlantic climate variability in CCSM3. *J Clim* 19:2451–2481
- Deser C et al (2012) ENSO and Pacific decadal variability in the community climate system model version 4. *J Clim* 25:2622–2651
- Du Y, Xie SP (2008) Role of atmospheric adjustments in the TIO warming during the 20th century in climate models. *Geophys Res Lett* 35:L08712. doi:10.1029/2008GL033631
- Ducet N, Le Traon PY, Reverdin G (2000) Global high resolution mapping of ocean circulation from TOPEX/Poseidon and ERS-1/2. *J Geophys Res* 105:19477–19498
- Duchon CE (1979) Lanczos filtering in one and two dimensions. *J Appl Meteorol* 18:1016–1022
- Feng M, McPhaden MJ, Lee T (2010) Decadal variability of the Pacific subtropical cells and their influence on the southeast

- Indian Ocean. *Geophys Res Lett* 37:L09606. doi:[10.1029/2010GL042796](https://doi.org/10.1029/2010GL042796)
- Folland C, Renwick JA, Salinger MJ, Mullan AB (2002) Relative influences of the Interdecadal Pacific Oscillation and ENSO on the South Pacific convergence zone. *Geophys Res Lett* 29:1643. doi:[10.1029/2001GL014201](https://doi.org/10.1029/2001GL014201)
- Gadgil S, Joseph PV, Joshi NV (1984) Ocean-atmosphere coupling over monsoon regions. *Nature* 312:141–143
- Garreaud R, Battisti D (1999) Interannual (ENSO) and interdecadal (ENSO-like) variability in the Southern Hemisphere tropospheric circulation. *J Clim* 12:2113–2123
- Goddard L, Baethgen W, Kirtman B, Meehl GA (2009) The urgent need for improved models and predictions. *EOS* 90:343
- Graham NE, Barnett TP (1987) Sea surface temperature, surface wind divergence, and convection over tropical oceans. *Science* 238:657–659
- Hack JJ, Caron JM, Danabasoglu G, Oleson KW, Bitz C, Truesdale J (2006) CCSM–CAM3 climate simulation sensitivity to changes in horizontal resolution. *J Clim* 19:2267–2289
- Hamlington BD, Leben R, Nerem RS, Han W, Kim KY (2011) Reconstructing sea level using cyclostationary empirical orthogonal functions. *J Geophys Res* 116. doi:[10.1029/2011JC007529](https://doi.org/10.1029/2011JC007529)
- Han W (2005) Origins and dynamics of the 90-day and 30–60 day variations in the equatorial Indian Ocean. *J Phys Oceanogr* 35:708–728
- Han W, Webster PJ, Lin J, Fu R, Yuan D, Hu A (2008) Dynamics of intraseasonal sea level and thermocline variability in the equatorial Atlantic during 2002–2003. *J Phys Oceanogr* 38:945–967
- Han W, Meehl GA et al (2010) Patterns of Indian Ocean sea level change in a warming climate. *Nat Geosci*. doi:[10.1038/NNGEO901](https://doi.org/10.1038/NNGEO901)
- Hoerling M, Hurrell J, Kumar A, Terray L, Eischeid J, Pegion P, Zhang T, Quan X, Xu T (2011) On North American decadal climate for 2011–2020. *J Clim* 24. doi:[10.1175/2011JCLI4137.1](https://doi.org/10.1175/2011JCLI4137.1)
- Huang BH, Kinter JL (2002) The interannual variability in the TIO and its relations to El Niño–Southern Oscillation. *J Geophys Res* 107:3199. doi:[10.1029/2000JC001278](https://doi.org/10.1029/2000JC001278)
- Hurrell JW, Hack JJ, Phillips AS, Caron J, Yin J (2006) The dynamical simulation of the community atmosphere model version 3 (CAM3). *J Clim* 19:2162–2183
- Hurrell JW, Hack JJ, Shea D, Caron JM, Rosinski J (2008) A new sea surface temperature and sea ice boundary dataset for the community atmosphere model. *J Clim* 21:5145–5153
- Hurrell JW, Meehl GA, Bader D, Delworth T, Kirtman B, Wielicki B (2009) A unified approach to climate system prediction. *Bull Amer Meteor Soc* 90:1819–1832
- Ishii M, Kimoto M (2009) Reevaluation of historical ocean heat content variations with time-varying XBT and MBT depth bias corrections. *J Oceanogr* 65:287–299
- Johnson NC, Xie SP (2010) Changes in the sea surface temperature threshold for tropical convection. *Nat Geosci* 3(12):842–845
- Kalnay E et al (1996) The NCEP/NCAR 40-year reanalysis project. *Bull Am Meteorol Soc* 77:437–471
- Kaplan A, Cane M, Kushnir Y, Clement A, Blumenthal M, Rajagopalan B (1998) Analyses of global sea surface temperature 1856–1991. *J Geophys Res* 103:18567–18589
- Kleeman R, McCreary JP, Klinger BA (1999) A mechanism for generating ENSO decadal variability. *Geophys Res Lett* 26:1743–1746
- Klein SA, Soden BJ, Lau NC (1999) Remote sea surface temperature variations during ENSO: evidence for a Tropical Atmospheric Bridge. *J Climate* 12:917–932
- Köhl A, Stammer D (2008) Variability of the meridional overturning in the North Atlantic from the 50-year GECCO state estimation. *J Phys Oceanogr* 38:1914–1930
- Köhl A, Stammer D, Cornuelle B (2007) Interannual to decadal changes in the ECCO Global Synthesis. *J Phys Oceanogr* 37:313–337
- Kumar A, Hoerling MP (1998) On the specification of regional SSTs in AGCM simulations. *J Geophys Res* 103:8901–8907
- Kumar A, Hoerling MP (2003) The nature and causes for the delayed atmospheric response to El Niño. *J Clim* 16:1391–1403
- Kumar K, Hoerling MP, Rajagopalan B (2005) Advancing Indian monsoon rainfall predictions. *Geophys Res Lett* 32:L08704. doi:[10.1029/2004GL021979](https://doi.org/10.1029/2004GL021979)
- Kushnir Y, Seager R, Ting M, Naik N, Nakamura J (2010) Mechanisms of Tropical Atlantic SST influence on North American precipitation variability. *J Clim* 23. doi:[10.1175/2010JCLI3172.1](https://doi.org/10.1175/2010JCLI3172.1)
- Lee T, McPhaden MJ (2008) Decadal phase change in large-scale sea level and winds in the Indo-Pacific region at the end of the 20th century. *Geophys Res Lett* 35:L01605. doi:[10.1029/2007GL032419](https://doi.org/10.1029/2007GL032419)
- Leuliette EW, Willis JK (2011) Balancing the sea level budget. *Oceanography* 24(2):122–129. doi:[10.5670/oceanog.2011.32](https://doi.org/10.5670/oceanog.2011.32)
- Liebmann B, Smith CA (1996) Description of a complete (interpolated) outgoing longwave radiation dataset. *Bull Am Meteorol Soc* 77:1275–1277
- Liu Z (2012) Dynamics of Interdecadal climate variability: an historical perspective. *J Clim* 25:1963–1995. doi:[10.1175/2011JCLI3980.1](https://doi.org/10.1175/2011JCLI3980.1)
- Liu Z, Alexander M (2007) Atmospheric bridge, oceanic tunnel, and global climatic teleconnections. *Rev Geophys* 45:RG2005. doi:[10.1029/2005RG000172](https://doi.org/10.1029/2005RG000172)
- Livezey RE, Chen WY (1983) Statistical field significance and its determination by Monte-Carlo Techniques. *Mon Wea Rev* 111(1):46–59
- Lombard A, Garric G, Penduff T (2009) Regional patterns of observed sea level change: insights from a 1/48 global ocean sea-ice hindcast. *Ocean Dyn* 59:433–449
- Luo JJ, Sasaki W, Masumoto Y (2012) Indian Ocean warming modulates Pacific climate change. *Proc Natl Acad Sci* 109:18701–18706
- Mantua NJ, Hare SR, Zhang Y, Wallace JM, Francis RC (1997) A Pacific interdecadal climate oscillation with impacts on salmon production. *Bull Am Meteorol Soc* 78:1069–1079
- McCreary JP (1981) A linear stratified ocean model of the coastal undercurrent. *Philos Trans R Soc Lond* 302A:385–413
- McGregor S, Sen Gupta A, England MH (2012) Constraining wind stress products with sea surface height observations and implications for Pacific Ocean sea-level trend. *J Clim* 25:8164–8176
- McPhaden MJ, Zhang D (2002) Slowdown of the meridional overturning circulation in the upper Pacific Ocean. *Nature* 415:603–608
- McPhaden MJ, Zhang D (2004) Pacific Ocean circulation rebounds. *Geophys Res Lett* 31:L18301. doi:[10.1029/2004GL020727](https://doi.org/10.1029/2004GL020727)
- Meehl GA, Goddard L et al (2009) Decadal prediction: can it be skillful? *Bull Am Meteorol Soc* 90:1467–1484
- Meehl GA, Hu A (2006) Megadroughts in the Indian monsoon region and southwest North America and a mechanism for associated multidecadal Pacific sea surface temperature anomalies. *J Clim* 19:1605–1623
- Merrifield MA (2011) A shift in western tropical Pacific sea level trends during the 1990s. *J Clim* 24:4126–4138
- Merrifield MA, Maltrud ME (2011) Regional sea level trends due to a Pacific trade wind intensification. *Geophys Res Lett* 38:L21605. doi:[10.1029/2011GL049576](https://doi.org/10.1029/2011GL049576)
- Merrifield MA, Thompson PR, Lander M (2012) Multidecadal sea level anomalies and trends in the western tropical Pacific. *Geophys Res Lett* 39:L13602. doi:[10.1029/2012GL052032](https://doi.org/10.1029/2012GL052032)

- Meyssignac B, Salas y Melia D, Becker M, Llovel W, Cazenave A (2012) Tropical Pacific spatial trend patterns in observed sea level: internal variability and/or anthropogenic signature? *Clim Past Discuss* 8:349–389
- Milne GA, Gehrels WR, Hughes CW, Tamisiea ME (2009) Identifying the causes of sea-level change. *Nature Geosci* 2:471–478
- Minobe S (1997) A 50–70 year climatic oscillation over the North Pacific and North America. *Geophys Res Lett* 24:683–686
- Nerem RS, Chambers DP, Choe C, Mitchum GT (2010) Estimating mean sea level change from the TOPEX and Jason altimeter missions. *Mar Geod* 33:435–446
- Newman M, Compo GP, Alexander MA (2003) ENSO-forced variability of the Pacific decadal oscillation. *J Clim* 16:3853–3857
- Nicholls RJ (2011) Planning for the impacts of sea level rise. *Oceanography* 24(2):144–157. doi:[10.5670/oceanog.2011.34](https://doi.org/10.5670/oceanog.2011.34)
- Nidheesh AG, Lengaigne M, Vialard J, Unnikrishnan AS, Dayan H (2012) Decadal and long-term sea level variability in the tropical Indo-Pacific Ocean. *Clim Dyn*. doi:[10.1007/s00382-012-1463-4](https://doi.org/10.1007/s00382-012-1463-4)
- Nigam S, Shen HS (1993) Structure of oceanic and atmospheric low-frequency variability over the tropical Pacific and Indian Oceans. Part I: COADS observations. *J Clim* 6:657–676
- Okumura YM, Ohba M, Deser C (2011) A proposed mechanism for the asymmetric duration of El Niño and La Niña. *J Clim* 24:3822–3829
- Power S, Colman R (2006) Multi-year predictability in a coupled general circulation model. *Clim Dyn* 26:247–272
- Power S, Casey T, Folland C, Colman A, Mehta V (1999) Interdecadal modulation of the impact of ENSO on Australia. *Clim Dyn* 15:319–324
- Randall DA, Wood RA, Bony S et al (2007) Climate models and their evaluation, ch. 8. In: Solomon S, Qin D, Manning M et al (eds) *Climate change 2007: the physical science basis, contribution of working group I to the fourth assessment report of the intergovernmental panel on climate change*. Cambridge University Press, Cambridge, pp 589–662
- Rayner NA, Brohan P, Parker DE, Folland CK, Kennedy JJ, Vanicek M, Ansell T, Tett SFB (2006) Improved analyses of changes and uncertainties in marine temperature measured in situ since the mid-nineteenth century: the HadSST2 dataset. *J Clim* 19:446–469
- Schneider N, Cornuelle B (2005) The forcing of the Pacific Decadal Oscillation. *J Clim* 18:4355–4373
- Schubert SD, Suarez MJ, Pegion PJ, Koster RD, Bacmeister JT (2004) Causes of long-term drought in the U.S. Great Plains. *J Clim* 17:485–503
- Simmons A, Uppala S, Dee D, Kobayashi S (2007) ERA-Interim: new ECMWF reanalysis products from 1989 onwards. *ECMWF Newsllett* 110:25–35
- Solomon A, Goddard L, Kumar A et al (2011) Distinguishing the roles of natural and anthropogenically forced decadal climate variability: implications for prediction. *Bull Am Meteorol Soc*. doi:[10.1175/2010BAMS2962.1](https://doi.org/10.1175/2010BAMS2962.1)
- Sutton RT, Hodson DLR (2005) Atlantic Ocean forcing of North American and European summer climate. *Science* 309:115–118
- Timmermann A, McGregor S, Jin FF (2010) Wind effects on past and future regional sea level trends in the southern Indo-Pacific. *J Clim* 23:4429–4437
- Tokenaga H, Xie SP (2011) Wave- and anemometer-based sea surface wind (WASWind) for climate change analysis. *J Clim* 24:267–285
- Trenary L, Han W (2013) Local and remote forcing of decadal sea level and thermocline depth variability in the South Indian Ocean. *J Geophys Res Oceans* 118. doi:[10.1029/2012JC008317](https://doi.org/10.1029/2012JC008317)
- Trenberth KE et al (2007) Surface and atmospheric climate change. In: Solomon S, Qin D, Manning M et al (eds) *Climate change 2007: the physical science basis, contribution of working group I to the fourth assessment report of the intergovernmental panel on climate change*. Cambridge University Press, Cambridge, pp 235–336
- Vimont D (2005) The contribution of the interannual ENSO cycle to the spatial pattern of decadal ENSO-like variability. *J Clim* 18:2080–2092
- Waliser DE, Graham NE, Gautier C (1993) Comparison of the highly reflective cloud and outgoing longwave data sets for use in estimating tropical deep convection. *J Clim* 6:331–353
- Wu R, Kirtman BP, Pegion K (2006) Local air–sea relationship in observations and model simulations. *J Clim* 19:4914–4932
- Wunsch C, Ponte R, Heimbach P (2007) Decadal trends in sea level patterns: 1993–2004. *J Clim* 20:5889–5911
- Xie SP, Annamalai H, Schott FA, McCreary JP (2002) Structure and mechanisms of south Indian Ocean climate variability. *J Clim* 15:864–878
- Xie SP, Hu K, Hafner J, Tokenaga H, Du Y, Huang G, Sampe T (2009) Indian Ocean capacitor effect on Indo-western Pacific climate during the summer following El Niño. *J Clim* 22:730–747
- Zhang X, Church JA (2012) Sea level trends, interannual and decadal variability in the Pacific Ocean. *Geophys Res Lett* 39:L21701. doi:[10.1029/2012GL053240](https://doi.org/10.1029/2012GL053240)
- Zhang Y, Wallace JM, Battisti DS (1997) ENSO-like interdecadal variability: 1900–1993. *J Clim* 10:1004–1020